iScience

CellPress
OPEN ACCESS

Article

Cytosolic adaptation to mitochondria-induced proteostatic stress causes progressive muscle wasting

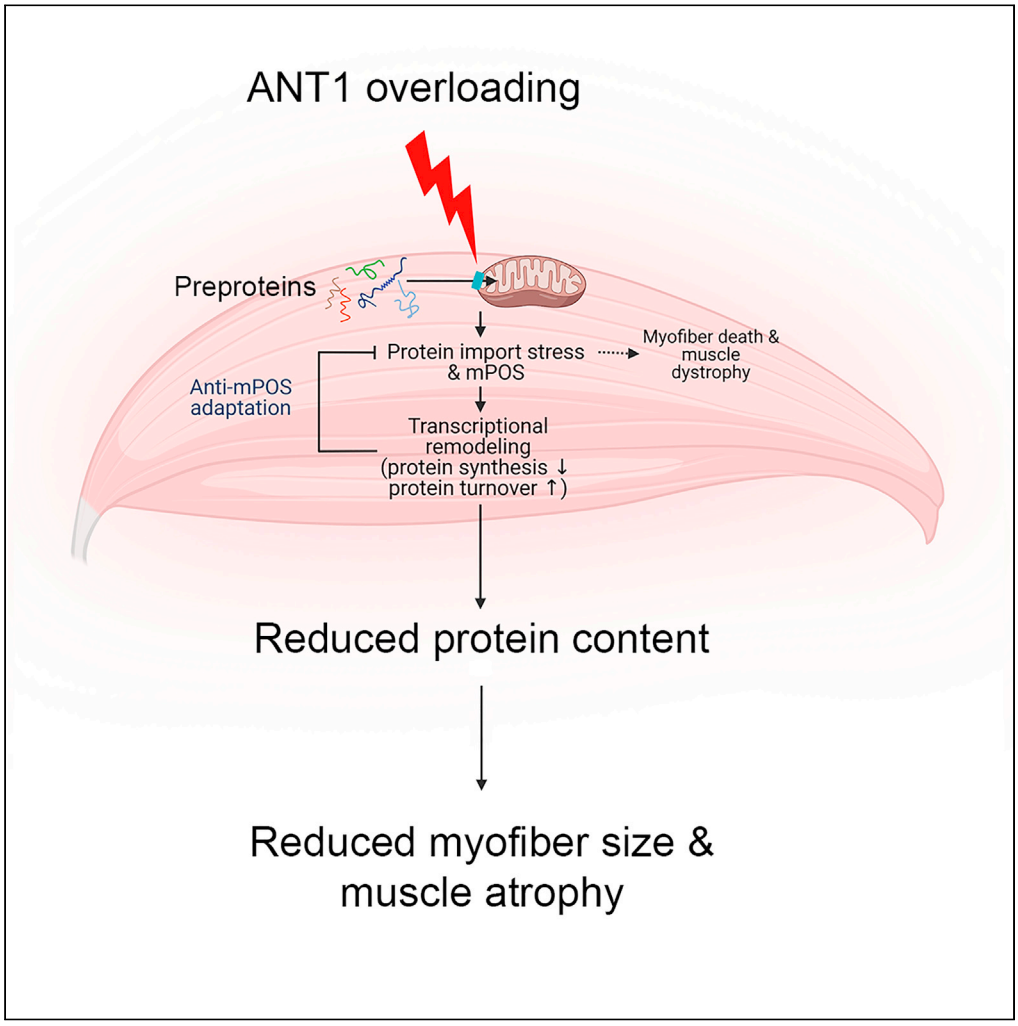

Xiaowen Wang, Frank A. Middleton, Rabi Tawil, Xin Jie Chen

Chenx@upstate.edu

Highlights

Ant1 overexpression causes progressive muscle wasting without affecting lifespan

ANT1 overloading saturates the mitochondrial protein import pathway to cause mPOS

Muscle responds to mPOS to repress the synthesis and increase turnover of proteins

Chronic adaptation to mPOS reduces myofiber size and muscle mass as a trade-off

Wang et al., iScience *25*, 103715
January 21, 2022
https://doi.org/10.1016/j.isci.2021.103715

iScience

CellPress
OPEN ACCESS

Article

Cytosolic adaptation to mitochondria-induced proteostatic stress causes progressive muscle wasting

Xiaowen Wang,[1] Frank A. Middleton,[2] Rabi Tawil,[3] and Xin Jie Chen[1,2,4,*]

SUMMARY

Mitochondrial dysfunction causes muscle wasting in many diseases and probably also during aging. The underlying mechanism is poorly understood. We generated transgenic mice with unbalanced mitochondrial protein loading and import, by moderately overexpressing the nuclear-encoded adenine nucleotide translocase, Ant1. We found that these mice progressively lose skeletal muscle. Ant1-overloading reduces mitochondrial respiration. Interestingly, it also induces small heat shock proteins and aggresome-like structures in the cytosol, suggesting increased proteostatic burden due to accumulation of unimported mitochondrial preproteins. The transcriptome of *Ant1*-transgenic muscles is drastically remodeled to counteract proteostatic stress, by repressing protein synthesis and promoting proteasomal function, autophagy, and lysosomal amplification. These proteostatic adaptations collectively reduce protein content thereby reducing myofiber size and muscle mass. Thus, muscle wasting can occur as a trade-off of adaptation to mitochondria-induced proteostatic stress. This finding could have implications for understanding the mechanism of muscle wasting, especially in diseases associated with *Ant1* overexpression, including facioscapulohumeral dystrophy.

INTRODUCTION

Muscle wasting (or atrophy) is defined by reduction of myofiber size and muscle mass and strength. It occurs during physiological aging, as well as in many diseases including neuromuscular degeneration, cancer, sepsis, diabetes, and cardiac failure. Muscle wasting is generally attributed to excessive protein degradation relative to protein synthesis (Cohen et al., 2015). Mitochondrial dysfunction is known to cause muscle wasting in mitochondrial myopathies (Chen et al., 2010). It is also proposed to play a role in the progressive muscle wasting process during aging (Calvani et al., 2013; Romanello and Sandri, 2016). However, how mitochondrial dysfunction contributes to muscle wasting and whether it is mechanistically linked to the loss of protein homeostasis are unclear. Interestingly, accumulating evidence indicates that merely reducing mitochondrial respiration or ATP export, along with elevated oxidative stress, has little or limited effect on muscle mass homeostasis during aging (Lustgarten et al., 2009, 2011; Morrow et al., 2017; Zhang et al., 2013). These observations raise the possibility that mitochondria may affect muscle mass homeostasis by mechanisms additional to or distinct from bioenergetic defect and oxidative stress.

Mitochondria are multifunctional. Mitochondrial abnormalities have been shown to affect cell fitness and survival by disrupting many processes that are not directly related to oxidative phosphorylation (OXPHOS). These processes include, but are not limited to, protein import, proteostatic signaling, metabolic remodeling, toxic metabolite accumulation, apoptosis, phospholipid synthesis, calcium homeostasis, redox balance maintenance, iron-sulfur cluster/heme biosynthesis, inflammation, cell-non-autonomous signaling, and epigenetic regulation (Coyne and Chen, 2018; Hunt et al., 2019; Naresh and Haynes, 2019; Nunnari and Suomalainen, 2012; Rugarli and Langer, 2012; Topf et al., 2016; Veatch et al., 2009; Wang, 2001; West et al., 2015; Zhang et al., 2018). Our recent studies demonstrated that various forms of mitochondrial damage, including intra-mitochondrial protein misfolding and reduced protein quality control, can directly trigger cytosolic proteostatic stress and cell death, a phenomenon named mitochondrial precursor overaccumulation stress (mPOS) (Wang and Chen, 2015). mPOS is characterized by reduced protein import and the toxic accumulation of unimported mitochondrial precursors/preproteins in the cytosol. Other studies uncovered cellular responses to defects in the mitochondrial protein import machinery. In yeast, mitochondrial protein import stress activates different cytosolic mechanisms including the Unfolded

[1]Department of Biochemistry and Molecular Biology, State University of New York Upstate Medical University, Syracuse, NY 13210, USA

[2]Department of Neuroscience and Physiology, State University of New York Upstate Medical University, Syracuse, NY 13210, USA

[3]Department of Neurology, University of Rochester, Rochester, NY 14642, USA

[4]Lead contact

*Correspondence: Chenx@upstate.edu

https://doi.org/10.1016/j.isci.2021.103715

Protein Response activated by mistargeting of proteins (UPRam), mitochondrial protein Translocation-Associated Degradation (mitoTAD), and mitochondrial Compromised Protein import Response (mitoCPR). These adaptive responses stimulate proteasomal degradation of unimported proteins and the removal of clogged preproteins on the mitochondrial surface (Martensson et al., 2019; Weidberg and Amon, 2018; Wrobel et al., 2015). Genes encoding cytosolic chaperones are also activated to counteract proteostatic stress in the cytosol (Boos et al., 2019). Furthermore, mitochondrial protein import stress also induces the nuclear and mitochondrial translocation of specific cellular factors to reprogram gene expression and restore cellular homeostasis (Lin and Haynes, 2016; Nargund et al., 2012; Poveda-Huertes et al., 2020). Currently, it is yet to be determined as to whether mPOS occurs in animals, how mammalian cells respond to mPOS *in vivo*, and whether mPOS and anti-mPOS signaling affect the homeostasis and function of specific tissues such as the skeletal muscle.

In this report, we show that a 2-fold increase in the expression of the mitochondrial carrier protein, Ant1, is sufficient to cause mitochondrial protein overloading relative to import capacity. This results in cytosolic proteostatic stress in the skeletal muscle. Interestingly, we found that, in response to the proteostatic burden, the transgenic muscles drastically remodeled the transcriptome. This ultimately unbalances protein synthesis and degradation in the cytosol, which likely contributes to the severe muscle wasting phenotype.

RESULTS

Moderate *Ant1* overexpression causes progressive muscle wasting

To learn whether mitochondrial protein import is saturable *in vivo* and to determine the physiological consequences of protein import stress, we generated transgenic mice overexpressing *Ant1*, encoding a nuclear-encoded mitochondrial carrier protein primarily involved in ADP/ATP exchange across the mitochondrial inner membrane (IMM). *Ant1*-overexpression is associated with facioscapulohumeral dystrophy (FSHD) (Gabellini et al., 2002; Laoudj-Chenivesse et al., 2005). An earlier study reported the use of transgenic mice expressing *Ant1* cDNA from the human α-skeletal actin promoter as a potential model of FSHD (Gabellini et al., 2006). These mice did not develop muscle pathology. However, that study failed to examine whether or not the ANT1 protein was actually overexpressed compared with control animals, which was a considerable limitation given that ANT1 is highly abundant in muscle mitochondria (Brand et al., 2005). Thus, whether *Ant1* overexpression does, or does not, cause muscle pathology remains undetermined. To address this, we generated *Ant1*-transgenic mice using the *Ant1* genomic locus and its native promoter (Figure 1A). We obtained two independent hemizygous transgenic founders (hereafter referred to as $Ant1^{Tg}$/+). Both were kyphotic (Figures S1A and S1B). We then mainly focused our studies on one of the transgenic lines. In the 16 successive generations of crosses to the wild type, ~50% of progeny inherited the $Ant1^{Tg}$ allele, which suggests single locus integration of the transgene. Quantitative PCR showed that *Ant1* copy number is increased by an average of 4.35-fold in the transgenic mice compared with the wild type (Figure S1C). Thus, 6–7 copies of the transgene are likely integrated in tandem into a single chromosomal site. RNA-seq analysis revealed that Ant1 transcripts are increased by 3.3-fold in the transgenic muscles (see below), and detailed analysis of the *Ant1* transcripts does not support the presence of mutant variants of the gene (Table S1). In the transgenic mice, the level of ANT1 protein is increased by only 2-fold in the skeletal muscles (Figures 1B and 1C). As expected, ANT1 is increased in mitochondria in the transgenic relative to the wild-type skeletal muscle (Figure S1D). ANT1 is also increased in the cytosol of the transgenic muscles compared with the wild type, which suggests incomplete import. Proteinase K protection assay showed that, like in the wild type, the imported ANT1 in the transgenic muscles is correctly targeted to the inner membrane (Figure S1E).

We found that the *Ant1*-transgenic (Tg) mice have reduced body weight. The animals cease to gain body weight at the age of 10–12 weeks, with males being more affected than females (Figures S2A and S2B). Food intake by the $Ant1^{Tg}$/+ mice is not reduced compared with wild-type controls (Figure S2C). The transgenic animals have a normal body length at the age of 6 months (Figure 1D), suggesting that there is no major developmental defect. Consistent with the kyphotic body morphology, micro-computed tomography (CT) confirmed that $Ant1^{Tg}$/+ mice have increased spinal curvature (Figure 1E). These mice develop gait abnormalities from the age of 6 months, which progressively deteriorates during aging (Figure 1F; Videos S1–S3). Along with body weight loss (Figure 1G), quantitative magnetic resonance analysis revealed that the male and female transgenic mice lose lean mass by 26.64% and 24.18%, respectively, at 6 months and by 36.28% and 35.01%, respectively, at 12 months of age (Figure 1H). At 14 months, quadriceps and

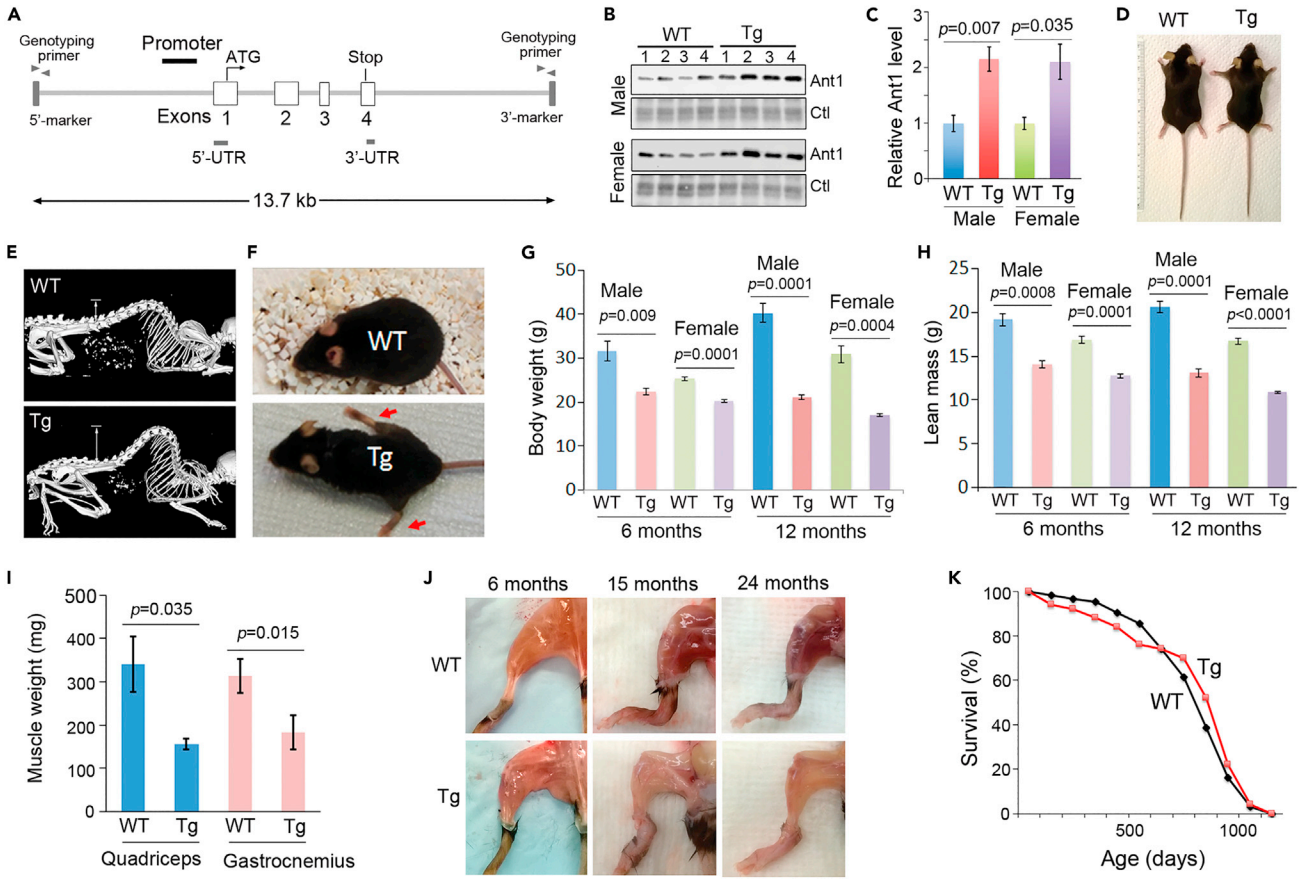

Figure 1. Moderate *Ant1* overexpression causes progressive muscle wasting without affecting the lifespan

(A) Schematic showing the genomic clone of the mouse *Ant1* gene, which was used to generate *Ant1*-transgenic mice.

(B and C) Steady-state levels of ANT1 in quadriceps muscle from transgenic (Tg) and wild-type (WT) littermates at age 6 months (n = 4/genotype/sex), as determined by western blot. Error bars represent SEM, and *p* values were calculated by unpaired Student's t test. Ctl, total protein control.

(D) Body length at 6 months.

(E) Micro-CT scanning showing kyphosis at 6 months.

(F) Gait abnormalities at 19 months.

(G and H) Body weight and lean mass at 6 and 12 months (n = 4/genotype/sex). Error bars represent mean ± SEM, and *p* values were calculated by unpaired Student's t test.

(I) Loss of quadriceps and gastrocnemius muscles in males at 14 months (n = 3/genotype). Error bars represent standard deviations, and *p* values were calculated by unpaired Student's t test.

(J) Progressive hindlimb muscle wasting.

(K) Lifespan of $Ant1^{Tg}$/+ mice (n = 50) compared with wild-type controls (n = 62).

gastrocnemius muscles are reduced by 54.13% and 41.84%, respectively (Figure 1I). Skeletal muscle becomes severely atrophic at 2 years of age (Figure 1J). Interestingly, the overall lifespan of the $Ant1^{Tg}$/+ mice is little affected compared with the wild-type controls (Figure 1K). This facilitated us to learn how mitochondrial protein import stress might affect muscle homeostasis across the lifespan.

To further support the idea that moderate overloading of ANT1 induces muscle atrophy, we performed histological analysis of the $Ant1^{Tg}$/+ and age-matched wild-type mice. We found that the $Ant1^{Tg}$/+ mice have drastically decreased myofiber size and increased myofiber size variability (Figures 2A–2C; Figures S3A and S3B). The average myofiber diameter is reduced by 26.18% and 49.46% at age 12 and 20 months, respectively (Figure S3B). Round- and angular-shaped myofibers and mild increase of endomysial connective tissues were observed in the *Ant1*-transgenic muscles (Figure 2A; Figures S3C–S3F). No myofiber type grouping was observed in muscle samples stained for mitochondrial activities (Figure S4), suggesting the lack of chronic neuropathy. Interestingly, we found that the $Ant1^{Tg}$/+ muscles have increased basophilic

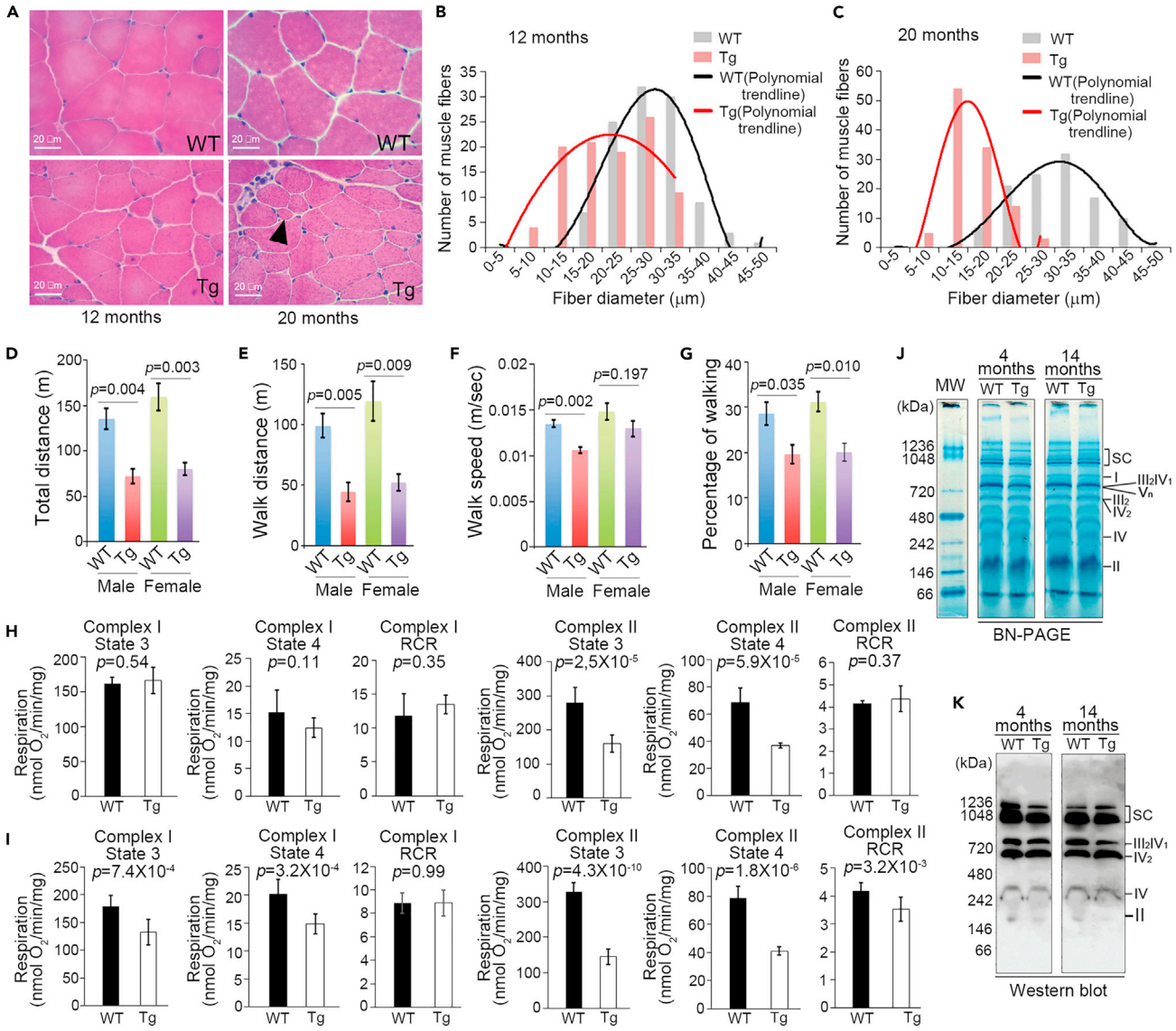

Figure 2. Histological, behavioral, and bioenergetic analyses of *Ant1*^{Tg}/+ mice

(A) H&E staining of quadriceps muscles. Arrowhead denotes a rounded small myofiber.

(B and C) Muscle fiber size distribution at the age of 12 and 20 months, respectively.

(D–G) Home cage activity of 1-year-old *Ant1*^{Tg}/+ and littermate control mice in the dark cycle (n = 4/genotype/sex). Note that we found no significant differences in home cage activity between *Ant1*^{Tg}/+ and control mice in the light cycle. Error bars represent SEM, and *p* values were calculated by unpaired Student's t test.

(H) Bioenergetic analysis of skeletal muscle mitochondria at 4 months of age. Error bars represent standard deviations of eight measurements with two pairs of *Ant1*^{Tg}/+ mice and littermate controls. *p* values were calculated by unpaired Student's t test. RCR, respiratory control ratio.

(I) Bioenergetic analysis of skeletal muscle mitochondria at 14 months of age. Error bars represent standard deviations of totally eight measurements from two pairs of *Ant1*^{Tg}/+ mice and littermate controls.

(J) BN-PAGE analysis of quadriceps mitochondria from 4- and 14-month-old mice. SC, supercomplexes. I–V, respiratory complexes I–V.

(K) Western blot analysis of BN-PAGE gel in (J) using antibodies against respiratory complexes.

stippling, which suggests the induction of possible acidic cellular components (Figure S5A). Moth-eaten myofibers were detected in the *Ant1*^{Tg}/+ muscles, as indicated by poor staining of NADH, succinate dehydrogenase (SDH), and cytochrome *c* oxidase (COX) (Figures S4 and S5B). The frequency of myofibers with central nuclei, commonly seen in regenerative myofibers, was not increased in the *Ant1*^{Tg}/+ muscles compared with controls (Figure S5C). It is likely that *Ant1* overexpression causes progressive muscle wasting mainly by processes that reduce myofiber size.

Consistent with muscle wasting and the myopathic phenotypes, the *Ant1*^{Tg}/+ mice have decreased home cage activities, reflected by reduction in total distance, walk distance, walk speed, and the percentage of walking (Figures 2D–2G). The effect on walk speed is less pronounced in females compared with males. Using the treadmill test, both male and female mice were found to have decreased exercise tolerance (Figures S2D–S2G). Taken together, the data indicate that moderate overloading of ANT1 on mitochondria is sufficient to reduce myofiber size and to cause progressive skeletal muscle wasting and exercise intolerance.

Mitochondrial respiration in *Ant1*^{Tg}/+ muscles

To understand the mechanism by which Ant1 overexpression causes muscle wasting, we first determined mitochondrial respiration in *Ant1*^{Tg}/+ compared with control muscles. At 4 months of age, complex I-driven state 3 and state 4 respiratory rates are comparable between *Ant1*^{Tg}/+ and wild-type muscles. Complex II-based state 3 and state 4 respiratory rates in *Ant1*^{Tg}/+ muscles are reduced by 42.98% and 46.45%, respectively, with the overall respiratory control ratio (RCR) unchanged (Figure 2H). At 14 months, complex I and complex II-based state 3 respiratory rates in *Ant1*^{Tg}/+ muscles are reduced by 26.13% and 55.71%, respectively, with the RCR either unaffected or moderately reduced (Figure 2I). Consistent with these data, blue native PAGE showed that the overall assembly of respiratory complexes and supercomplexes does not appear to be severely altered, with a subtle shift of the III_2IV_1 complex toward IV_2 in 14-month-old *Ant1*^{Tg}/+ muscles (Figures 2J and 2K). However, the levels of complex II is reduced in *Ant1*^{Tg}/+ muscles at both ages. These data demonstrate that moderate *Ant1*-overexpression causes progressive reduction of mitochondrial respiration. These effects likely result from reduced import of OXPHOS components and/or substrate transporters due to ANT1-induced import stress. Previous studies by others have shown that more severe bioenergetic deficiencies are insufficient to induce muscle wasting during aging (Lustgarten et al., 2011). We thus speculate that factors other than bioenergetic deficiencies may account for the *Ant1*-induced muscle wasting phenotype.

ANT1 overloading induces aggresome formation in the cytosol

Our previous studies have shown that overexpression of mitochondrial carrier proteins in human embryonic kidney HEK293T cells imposes a drastic proteostatic burden in the cytosol, as manifested by the formation of aggresomes that contain unimported mitochondrial proteins (Liu et al., 2019). To ascertain whether *Ant1* overexpression in *Ant1*^{Tg}/+ muscles causes protein import stress and the formation of cytosolic protein aggregates and/or aggresome-like structures *in vivo*, we directly examined the *Ant1*^{Tg}/+ and control muscles by transmission electron microscopy. Indeed, we detected various forms of aggresome-like structures in the cytosol of *Ant1*^{Tg}/+ muscles (Figures 3B–3E and 3L–3P), which is a rare event in the wild type (Figures 3A and 3K; Figure S5D). These structures contain a single or multiple electron-dense patches of various sizes and shapes, which reassemble protein aggregates. Many of the aggregates are confined within membrane-bound vesicles that could arise from aggrephagy. These data support the idea that a 2-fold increase of ANT1 is sufficient to saturate the mitochondrial protein import machinery, which likely causes the accumulation and aggregation of unimported mitochondrial proteins in the cytosol.

ANT1 overloading activates genes involved in mitochondrial protein import and proteostasis and genes encoding cytosolic small heat shock family B chaperones

We speculated that the formation of aggresome-like structures is an adaptive process to counteract the proteostatic stress caused by the overaccumulation of unimported mitochondrial proteins in the *Ant1*^{Tg}/+ muscles. To provide further support, we analyzed the transcriptome of *Ant1*^{Tg}/+ skeletal muscles by RNA-seq. We identified 24,106 genes (Figure 4A; Table S2), among which 2,729 genes were differentially expressed in the *Ant1*^{Tg}/+ versus wild-type (WT) muscles (one-way ANOVA, $q < 0.01$; Table S2). Among these genes, 196 were upregulated and 54 downregulated at the $\pm$2.0-fold level and 42 genes were upregulated and 6 downregulated at the $\pm$4-fold level (Figure 4B; Table S3; Figure S6). The highly upregulated genes participate in biological functions including integrated stress response (ISR, see below), amino acid transport and metabolism (e.g., *SLC7A1*, *SLC7A5* and *ASNS*), one-carbon metabolism (e.g., *MTHFD2* and *PSAT1*), and myokine signaling (e.g., *FGF21* and *GDF15*). Activation of these genes has previously been reported in various cell and mouse models of mitochondrial stresses and diseases (Bao et al., 2016; Dogan et al., 2014; Ishikawa et al., 2009; Kuhl et al., 2017; Nikkanen et al., 2016; Ost et al., 2015; Tyynismaa et al., 2010). Gene set enrichment analysis (GSEA) revealed that expression of genes involved in various proteostatic processes in the cytosol is altered (Table S4). Many of these genes participate in mRNA processing, ribosomal biogenesis, protein translation, and amino acid metabolism. Genes directly involved in oxidative

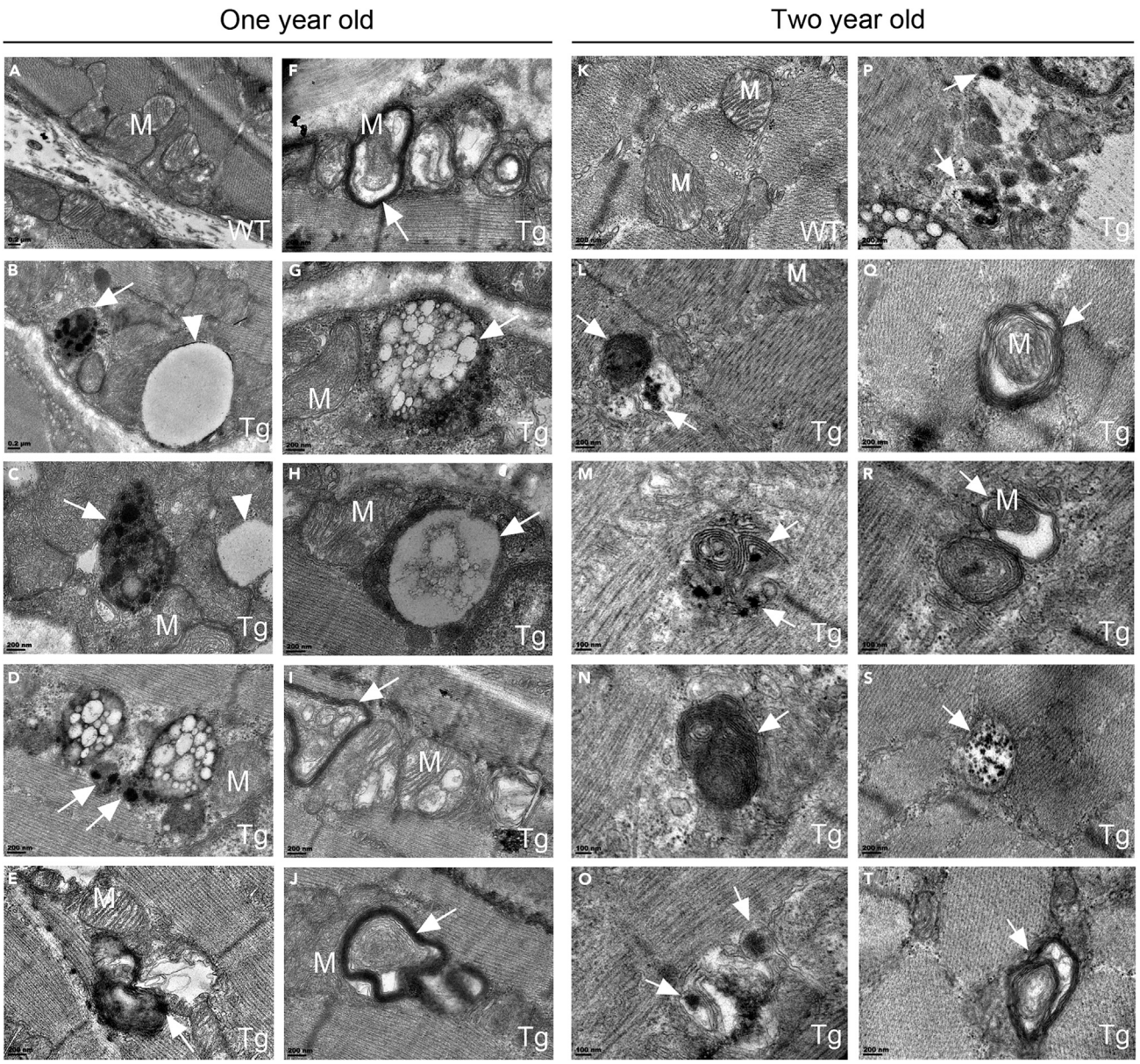

Figure 3. Transmission electron microscopy of quadriceps muscles from *Ant1*^{Tg}/+ (Tg, panels B–J and L–T) and wild-type (WT, panels A and K) mice at age 1 and 2 years

M, mitochondria. Arrows denote aggresome/lysosome-like structures that contain electron-dense aggregates (B–E; L–P), mitophagic vacuoles (F, Q, and R), multivesicular vacuoles (G and H), multilamellar vesicles (I, J, and T), and structures resembling glycophagy body (S). Arrowheads denote structures resembling lipid droplets.

phosphorylation and anti-oxidant defense were not over-represented among the upregulated genes in the *Ant1*^{Tg}/+ muscles. Instead, we found that several upregulated genes in the "mitochondrial inner membrane" gene ontology group are involved in mitochondrial protein import, including *TOMM40, TOMM5, TOMM34, TIMM8A1, TIMM10, TIMM44, HSPA9, DNAJA3,* and *CHCHD10* (Figure 4C). This supports the existence of a retrograde regulatory mechanism in the skeletal muscle that promotes mitochondrial protein import. *HSPE1*, *LONP1*, and *CLPP*, encoding the mitochondrial Hsp10, the Lon protease, and the proteolytic subunit of the Clp peptidase in the matrix, respectively, were also upregulated (Figure 4C). This is reminiscent of the mitochondrial Unfolded Protein Response (mtUPR) and mitochondrial Compromised Protein import Response (mitoCPR) mechanisms that are activated to cope with increased proteostatic stress inside the mitochondria of *C. elegans* and *S. cerevisiae* (Lin and Haynes, 2016; Weidberg and Amon, 2018).

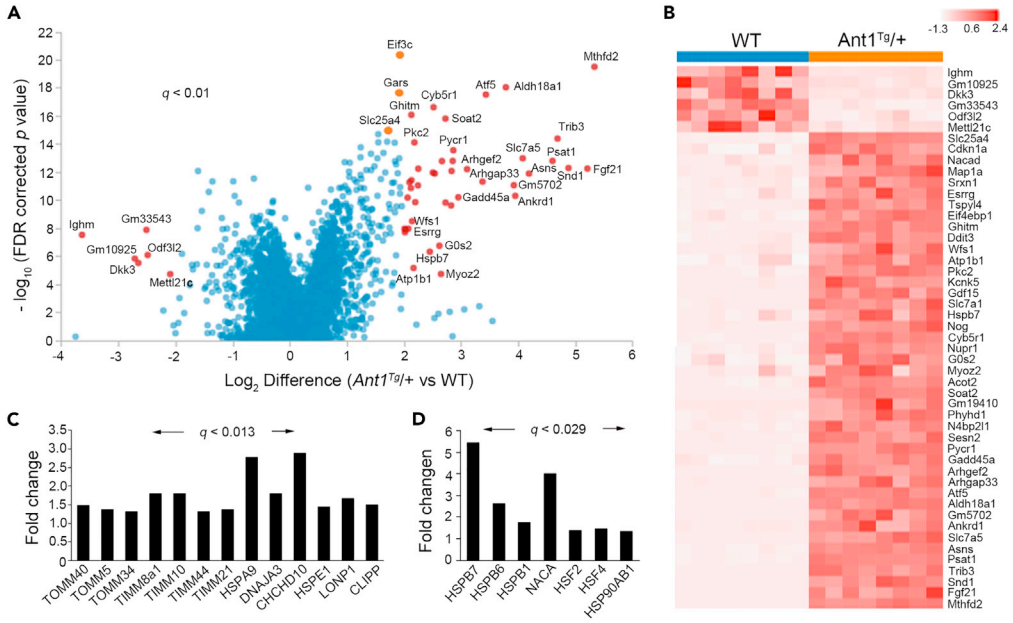

Figure 4. Transcriptional responses to *Ant1* overexpression determined by RNA-seq (n = 4/genotype/sex)

(A) Volcano plot with limma-based *p* values. Genes with 4-fold changes at FDR <0.01 are indicated in red. Additional genes of interest are noted in orange. RNA samples were extracted from quadriceps muscle at the age of 6 months (one-way ANOVA, $q < 0.01$).

(B) Hierarchical clustering heatmap of 48 genes with 4-fold changes in *Ant1*^{Tg}/+ versus WT mice, at FDR <0.01. *Ant1* (Slc25a4) is included for comparative purposes.

(C) Upregulation of genes involved in mitochondrial protein import and proteostasis.

(D) Upregulation of genes encoding cytosolic chaperones.

In addition to the genes involved in mitochondrial protein import and proteostasis, we found that genes encoding specific cytosolic chaperones and the heat shock transcription factor 2 and 4 (Hsf2 and Hsf4) are upregulated in the *Ant1*^{Tg}/+ muscles (Figure 4D). Notably, genes encoding the small heat shock family B chaperones such as HSPB7, HSPB6, and HSPB1 are activated. These ATP-independent chaperones are known to provide protection against muscular cell dysfunction and atrophy and are involved in many neurological, muscular, and age-related diseases in humans (Carra et al., 2017). Functionally, the small cytosolic chaperones constitute the first line of cellular defense against proteostatic stress through their activities in capturing early-unfolding states of proteins and in promoting the formation of aggregates to alleviate cytotoxicity (Mogk et al., 2019). Finally, we found that *Naca* and *Hsp90AB1* are activated in *Ant1*^{Tg}/+ muscles. *Naca* encodes a subunit of the nascent polypeptide-associated complex (NAC) that plays a role of chaperone under proteostatic stress (Kirstein-Miles et al., 2013). *Hsp90AB1* encodes a member of the HSP90 family chaperones. Taken together, our data suggest that *Ant1* overexpression causes mitochondrial protein import stress, which subsequently induces proteostatic stress in the cytosol. We speculate that the small heat shock proteins and other chaperones may play a role in the deposition of unimported mitochondrial proteins.

Transcriptomic remodeling to suppress protein synthesis in *Ant1*^{Tg}/+ muscles

GSEA of the RNA-seq data revealed changes to expression of genes in several biosynthetic pathways (Table S4). Particularly, genes involved in mRNA processing, amino acid biosynthesis, aminoacyl-tRNA biosynthesis, and ribosomal biogenesis are significantly over-represented in the *Ant1*^{Tg}/+ muscles. These changes are typical signatures of amino acid starvation response, possibly reflecting a protein depletion stress in the muscle. Consistent with this, several lines of evidence suggest that the transcriptome of the *Ant1*^{Tg}/+ muscles is remodeled to suppress global protein translation, likely as an adaptive response to counteract proteostatic stress in the cytosol. First, *Atf4, Atf5, Ddit3,* and *Nupr1* are strongly activated (Figure 5A). These genes are known to be upregulated as an important regulatory circuit in the ISR. ISR is an elaborating signaling network that is stimulated by diverse cellular stresses to decrease global protein

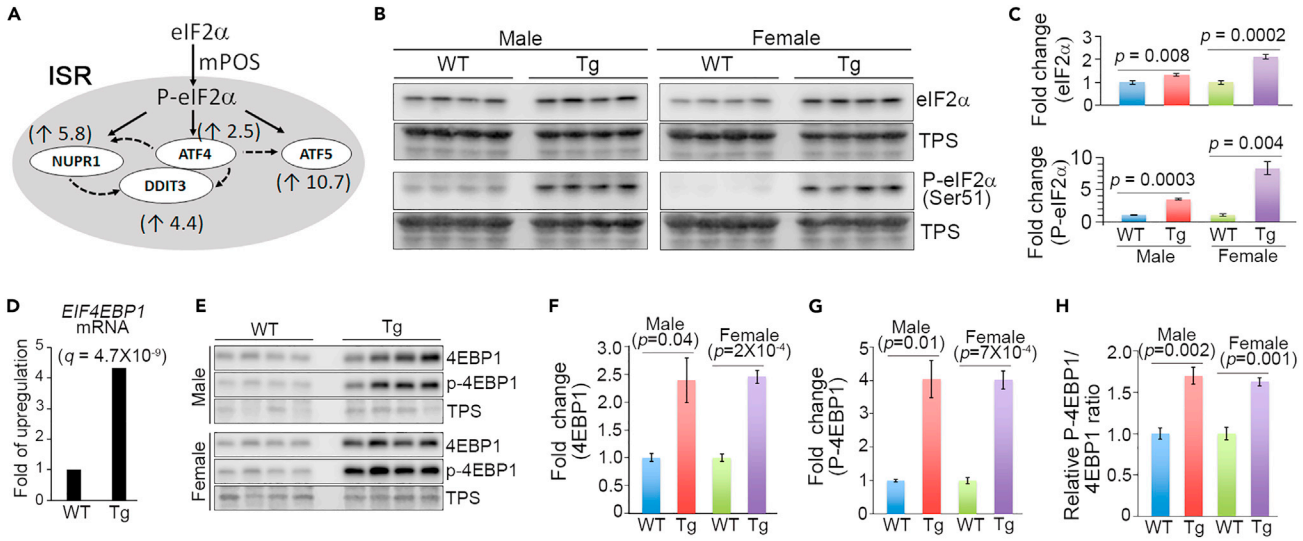

Figure 5. Activation of integrated stress response (ISR) and transcriptional upregulation of *Eif4ebp1* in *Ant1*^{Tg}/+ (Tg) muscles compared with wild-type (WT) controls (n = 4/genotype/sex)

(A) Upregulation of ISR genes in *Ant1*^{Tg}/+ muscles. Fold changes in transcription are indicated in the parentheses. Solid lines represent translational activation, and dashed lines denote transcriptional activation.

(B and C) Western blot showing the levels of eIF2α and its phosphorylated form, P-eIF2α (Ser51), in *Ant1*^{Tg}/+ and wild-type mice at age 6 months. The signals were quantified using the LI-COR Biosciences Imager. TPS, total protein staining.

(D) Transcriptional activation of *Eif4ebp1* in *Ant1*^{Tg}/+ muscles as revealed by RNA-seq.

(E–G) Western blot showing the upregulation of 4EBP1 protein and its phosphorylated form, P-4EBP1.

(H) The relative ratio between phosphorylated and non-phosphorylated forms of 4EBP1 in *Ant1*^{Tg}/+ muscles compared with wild-type controls. Error bars represent mean ± SEM, and *p* values were calculated by unpaired Student's t test.

synthesis and to activate selected genes in the benefit of cellular recovery (Pakos-Zebrucka et al., 2016). Supporting this, we found that phosphorylation of eIF2α, a central step in ISR activation, is significantly increased in *Ant1*^{Tg}/+ muscles (Figures 5B and 5C). This eIF2α phosphorylation likely upregulates *Atf4*, *Atf5*, *Ddit3*, and *Nupr1* (Figure 5A), by promoting cap-independent translation of these transcriptional factors followed by a feedforward loop of transcriptional activation (Pakos-Zebrucka et al., 2016). Activation of these transcriptional factors has been observed in various models of mitochondrial stress (Dogan et al., 2014; Hunt et al., 2019; Khan et al., 2017; Silva et al., 2009; Zurita Rendon and Shoubridge, 2018). More importantly, phosphorylated eIF2α is known to directly suppress global protein synthesis by interfering with cap-dependent translation initiation, in response to various stresses including mitochondrial damage (Baker et al., 2012; Quiros et al., 2017).

Second, we found that the transcription of *Eif4ebp1* (or *4ebp1*) is drastically increased in *Ant1*^{Tg}/+ muscles (Figure 5D). Consequently, the levels of both 4EBP1 and its phosphorylated form, P-4EBP1, are increased (Figures 5E–5G). Given that the non-phosphorylated 4EBP1 actively binds eIF4E to represses protein translation, transcriptional activation of *Eif4ebp1* would be expected to repress protein translation in the *Ant1*^{Tg}/+ muscle, although the P-4EBP1/4EBP1 ratio is increased in the transgenic mice (Figure 5H). It is noteworthy that 4EBP1 is a substrate of several protein kinases including the mechanistic target of rapamycin (mTOR) kinase. We found that the phosphorylation of Rps6 kinase (S6K), another substrate of mTOR, is not significantly increased in the *Ant1*^{Tg}/+ muscles (Figures S7A–S7E). Therefore, the data do not support a global increase of mTOR signaling.

Activation of multiple protein degradation pathways in *Ant1*^{Tg}/+ muscles

Our RNA-seq analysis also revealed that several proteolytic pathways are activated in *Ant1*^{Tg}/+ muscles. First, we found that transcription of genes encoding proteasomal subunits are upregulated (Figure S7F). *NFE2L1* and *NFE2L2*, involved in the transcription of proteasomal genes, are also activated (Figure S7G). Accordingly, proteasome-associated trypsin-like activity is increased in the *Ant1*^{Tg}/+ muscles (Figure 6A). We found that the overall levels of ubiquitinated proteins, and p62 that promotes the formation and

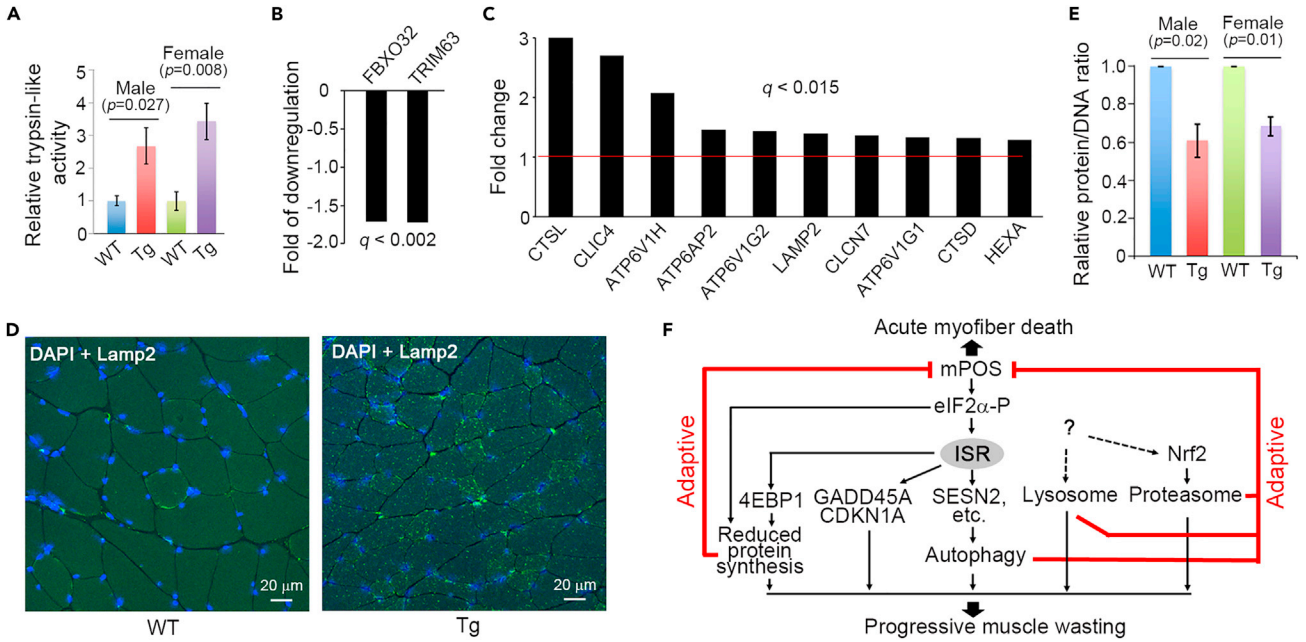

Figure 6. Activation of cytosolic proteolytic pathways and decrease of protein content in *Ant1*^{Tg}/+ muscles

(A) Trypsin-like activity associated with the proteasome in *Ant1*^{Tg}/+ quadriceps muscles. Error bars represent SEM of four male and female mice with four measurements from each mouse. The *p* values were calculated by unpaired Student's t test.

(B) Transcriptional down-regulation of *Fbxo32* and *Trim63uscles*^{Tg}/+ *quadriceps muscles.*

(C) Transcriptional upregulation of genes encoding lysosomal function.

(D) Immunofluorescence detection of LAMP2-positive structures in cross sections of quadriceps from *Ant1*-transgenic and control mice. Blue, DAPI-stained nuclei; green, LAMP2-positive structures.

(E) Relative protein/DNA ratio in 6-month-old quadriceps muscles (n = 4/genotype/sex).

(F) A model for muscle wasting. mPOS-induced proteostatic adaptations unbalance protein synthesis and degradation, which may contribute to progressive muscle wasting as a trade-off. Red lines represent adaptive processes to counteract mPOS, and the dashed lines denote an unknown transcriptional activation mechanism.

removal of ubiquitinated and aggregated proteins, are not increased in the *Ant1*^{Tg}/+ muscles (Figures S7H–S7K). It is likely that the activation of proteasomal function, perhaps together with other proteolytic processes (see below), can efficiently prevent the accumulation of ubiquitinated proteins. In acute models of muscle atrophy, *Fbxo32* and *Trim63*, encoding the MAFBx/atrogin-1 and MuRF1 ubiquitin ligases, respectively, are frequently upregulated (Bonaldo and Sandri, 2013). Interestingly, we found that these genes are instead downregulated in the *Ant1*^{Tg}/+ muscles (Figure 6B). This observation suggests that muscle wasting in *Ant1*^{Tg}/+ mice is independent of FBXO32 and TRIM63.

Second, we found that numerous genes involved in autophagy, cytoskeletal organization, and intracellular trafficking are upregulated in *Ant1*^{Tg}/+ muscles (Figures S7L and S7M). Among the most upregulated genes related to autophagy are *Sesn2* and *Stbd1*. SESN2 activates mitophagy (Kim et al., 2016; Kumar and Shaha, 2018). In accordance with this, we detected mitophagic structures in *ANT1*^{Tg}/+ but not control muscles (Figures 3F, 3Q, and 3R). STBD1 is a selective autophagy receptor for glycogen (Jiang et al., 2010), consistent with the presence of glycophagy-like structures in the *Ant1*^{Tg}/+ muscles (Figure 3S). *Arhgap33* and *Arhgef2* are the mostly activated genes in the cytoskeletal organization and intracellular trafficking gene group. These two genes encode a sorting nexin family member and a Rho-Rac guanine nucleotide exchange factor, respectively, which are involved in vesicular trafficking (Eisler et al., 2018; Krendel et al., 2002; Nakazawa et al., 2016). Our transmission electron microscopy analysis also revealed the presence of many vesicular structures of various morphologies in *Ant1*^{Tg}/+ muscles, which includes multivesicular vacuoles (Figures 3G and 3H) and multilamellar vesicles (Figures 3I, 3J, and 3T; Figure S5D). The origin of these membranous structures is yet to be further investigated.

Finally, we found that a group of genes encoding lysosomal function are upregulated in *Ant1*^{Tg}/+ muscles (Figure 6C). These include *Ctsl*, encoding the lysosomal cathepsin L protease. The levels of the lysosomal

Lamp1 and Lamp2 proteins are also increased (Figure S7N). Using immunofluorescence staining, we found that Lamp2-positive lysosomes and/or lysosome-derived structures are increased in the *Ant1*^{Tg}/+ muscles (Figure 6D; Figure S8; Videos S4 and S5), possibly reflecting the basophilic cellular components detected by H&E staining (Figure S5A).

Reduced protein content in *Ant1*^{Tg}/+ muscles

Excessive protein degradation relative to protein synthesis is the primary driver under many muscle wasting conditions (Bonaldo and Sandri, 2013). Given that multiple proteolytic pathways are activated, and that ISR and 4EBP1 are activated, which is well known to repress global protein translation, we speculated that the balance between protein synthesis and degradation may be disturbed to reduce overall protein content in the *Ant1*^{Tg}/+ muscles. This turned out to be the case. We found that the protein content is drastically reduced in the *Ant1*^{Tg}/+ muscles compared with wild-type controls (Figure 6E).

DISCUSSION

Muscle wasting occurs under many disease conditions and probably also during aging. A prevailing mechanism involves an imbalance between protein synthesis and degradation. When protein degradation exceeds synthesis, intracellular protein content is reduced. This directly reduces myofiber size and causes muscle mass loss (Bonaldo and Sandri, 2013). Mitochondrial dysfunction is known to cause muscle wasting in mitochondrial myopathic diseases (Chen et al., 2010). It is also proposed to contribute to sarcopenia (Calvani et al., 2013; Romanello and Sandri, 2016). However, how mitochondrial dysfunction triggers the atrophying process and whether it involves proteostatic imbalance are unknown. In this report, we established a novel mouse model of mitochondria-induced progressive muscle wasting that involves mitochondrial protein import stress by moderately overexpressing the ANT1 protein. As the lifespan of the animals is unaffected, the scope and mechanism of muscle wasting during aging can be investigated in detail.

We found that *Ant1* overexpression reduces mitochondrial respiration. Interestingly, it also induces cytosolic proteostatic stress (or mPOS), manifested by aggresome formation and the activation of small heat shock family B chaperones in the cytosol. Muscle cells respond to mPOS by activating multiple proteostatic pathways (Figure 6F). First, eIF2α phosphorylation is increased, which is well known to directly repress cap-dependent protein translation. Second, we observed the transcriptional activation of *Eif4ebp1*, which is a direct target of the ISR network (Juliana et al., 2017). This leads to the accumulation of both non-phosphorylated and phosphorylated forms of the protein, with the former acting as a repressor of protein translation. Third, we found that ANT1 overloading activates many genes involved in autophagy, vesicular trafficking, lysosomal biogenesis, and proteasomal function. Activation of these genes may be protective against proteostatic stress, by directly contributing to the formation of aggresomes and the clearance of unimported mitochondrial proteins. The autophagic gene *Sesn2* is directly activated by the ISR network (Garaeva et al., 2016). How the other autophagic genes are transcriptionally activated is yet to be determined. We found that ANT1-induced proteostatic stress also activates genes involved in proteasomal function, reminiscent of the UPRam mechanism observed in yeast when cells are challenged by mitochondrial protein import stress (Topf et al., 2016; Wrobel et al., 2015). Taken together, our data revealed that the skeletal muscle responds to ANT1-induced mitochondrial protein import stress and the resulting cytosolic proteostatic stress by both suppressing protein synthesis and by promoting protein sequestration and degradation. We propose that activation of these adaptive processes collectively remodels cytosolic proteostasis to avoid acute myofiber death. As a trade-off, these chronic adaptations may contribute to the reduction of the overall protein content, which ultimately reduces myofiber size and causes muscle wasting (Figure 6F).

Our study supports a novel mechanism of muscle wasting, caused by an imbalance between mitochondrial protein load and import capacity. Although *Ant1* is a highly expressed gene, it is intriguing to observe that a 2-fold increase in the level of a single protein suffices to induce drastic proteostatic and metabolic adaptations in the cytosol. This observation underscores the vulnerability of the balance between mitochondrial protein loading and import capacity *in vivo*. Because unbalanced mitochondrial protein loading and import is expected to occur under many pathophysiological conditions, our finding could have potential implications for other myopathic diseases involving mitochondrial stress. In addition to mutations in the core protein import machinery that directly reduce protein import capacity, overexpression of nuclear-encoded mitochondrial proteins may lead to preprotein overloading and saturation of the import machinery. IMM proteostatic stress and conditions affecting the generation and maintenance of membrane potential

may indirectly reduce protein import efficiency. Under these conditions, the preprotein chaperoning and delivery systems in the cytosol become saturated. The levels of import receptors/channels become limited for the mitochondrial translocation of the excessive preproteins. As cytosolic aggresomes are readily detected, our data would also suggest that the cytosol has a limited capacity in degrading unimported mitochondrial preproteins in the skeletal muscle. In addition to the skeletal muscle, *Ant1* is also expressed in other tissues including the central nervous system. Despite the severe muscle wasting phenotype, we did not observe obvious phenotypes that may suggest neurodegeneration in the $Ant1^{Tg}$/+ mice. This is consistent with the observation that the overall lifespan of the transgenic animals is unaffected. It is possible that the neuronal tissues have a higher capacity than the skeletal muscle in handling mitochondrial protein import stress. The central nervous system expresses both *Ant1* and *Ant2*. Thus, it is also possible that the total level of ANT1 is not sufficient to saturate the protein import machinery and to cause cytosolic stress to the same extent as in the skeletal muscle. This question needs to be addressed in future studies.

We found that *Ant1*-induced proteostatic stress leads to eIF2α phosphorylation and ISR activation. ISR activation has been previously documented in various models of mitochondrial stress (Baker et al., 2012; Dogan et al., 2014; Ishikawa et al., 2009; Khan et al., 2017; Kuhl et al., 2017; Quiros et al., 2017; Silva et al., 2009; Zurita Rendon and Shoubridge, 2018). What triggers eIF2α phosphorylation in $Ant1^{Tg}$/+ muscles remains unsolved. Our RNA-seq analysis did not detect the upregulation of anti-oxidant enzymes, which rules out the possibility that oxidative stress plays a major role in ISR activation. We found that complex II-based mitochondrial respiration is reduced in the $Ant1^{Tg}$/+ muscles at 4 and 14 months of age, whereas defect in complex I-based respiration is detected only at 14 months. We speculate that decreased mitochondrial respiration may result from an overall reduction in the import of OXPHOS components and/or substrate transporters when cells are challenged by ANT1 overloading and the saturation of the protein import machinery. It is noteworthy that our current bioenergetic studies are based on rather small sample sizes. More thorough studies are needed in future to consolidate these conclusions and particularly, to understand the seemingly preferential effect on complex II-based respiration. Given that severe bioenergetic defect has very limited effect on muscle mass homeostasis during aging (Lustgarten et al., 2009, 2011; Morrow et al., 2017; Zhang et al., 2013), it is unlikely that reduced ATP synthesis drives the severe muscle wasting phenotype in the $Ant1^{Tg}$/+ mice.

Four stress-sensing kinases are known to promote eIF2α phosphorylation. These are HRI (EIF2AK1), PKR (EIF2AK2), PERK (EIF2AK3), and GCN2 (EIF2AK4), which are activated by heme deficiency/heavy metals, viral infection, endoplasmic reticulum stress, and amino acid deficiency, respectively (Pakos-Zebrucka et al., 2016). ISR activation by mitochondrial stressors in HeLa cells seems to be independent of the four eIF2α kinases (Quiros et al., 2017). More recent studies showed that mitochondrial stress in cultured cells causes the release of the DELE1 protein, which in turn binds and activates the HRI kinase (Fessler et al., 2020; Guo et al., 2020). On the other hand, mitochondrial stress activates ISR via GCN2 in myoblasts but not in myotubes (Mick et al., 2020). It would be of great interest to determine whether ANT1 overloading induces eIF2α phosphorylation *in vivo* by any of these kinases or by an independent pathway.

In addition to the activation of multiple pro-atrophic proteostatic pathways in $Ant1^{Tg}$/+ muscles, it is relevant to note that Ant1 overloading also activates *Gadd45a* and *Cdkn1a* (Figure S7O), two additional targets downstream of the ISR network (Adams et al., 2017). *Gadd45a* and *Cdkn1a* encode the growth arrest and DNA-damage-inducible protein α, and the cyclin-dependent kinase inhibitor 1A (or p21), respectively. Both proteins promote muscle atrophy (Bongers et al., 2013; Ebert et al., 2012; Fox et al., 2014). GADD45A has also been shown to repress protein synthesis and activate proteolysis via an unknown mechanism. Thus, it is possible that *Gadd45a* activation also contributes to the muscle wasting phenotype in the $Ant1^{Tg}$/+ mice.

Our observation that a 2-fold increase of ANT1 is sufficient to cause severe muscle atrophy could have direct implications for human diseases such as FSHD and dilated cardiomyopathy that are associated with *Ant1* activation (Dorner et al., 1997; Gabellini et al., 2002; Kim et al., 2015; Laoudj-Chenivesse et al., 2005). FSHD is primarily linked to the ectopic expression of *Dux4* in the skeletal muscle. It encodes a transcription factor that is not normally expressed in somatic tissue (Statland and Tawil, 2011). In light of our study, it might be worth reexamining whether or not *Ant1* overexpression contributes to or modifies the course of this disease. Finally, our finding that mitochondrial protein import stress induces cytosolic proteostatic stress *in vivo* could also have implications for other clinical and subclinical conditions. Protein

import is an elaborate process (Chacinska et al., 2009). Protein import efficiency is expected to be directly or indirectly affected in many human diseases (Jackson et al., 2018; Kang et al., 2017; Koehler et al., 1999; Pacheu-Grau et al., 2018; Vukotic et al., 2017). Thus, our finding may help the better understanding of how mitochondrial damage affects tissue homeostasis in import-related diseases.

Limitation of study

We propose that imbalanced mitochondrial protein load and import is a robust mechanism that causes proteostatic stress in the cytosol (or mPOS) and drastic transcriptomic changes in the nucleus. The remodeling of nuclear transcriptome in the skeletal muscle is likely an anti-mPOS adaptation that contributes to the repression of global protein synthesis and the activation of proteolytic processes in favor of myofiber survival. Chronic adaptation comes with a trade-off as manifested by muscle atrophy. Despite these advances, our studies had limitations. First, we have not been able to isolate the aggresomes from the *Ant1*^{Tg}/+ muscles and determine if they contain unimported mitochondrial proteins. This is because subcellular fractionation does not allow separating the aggresomes from mitophagic structures that contain mitochondrial remnants/proteins. Second, further studies are needed to thoroughly evaluate the effect of ANT1 overloading on mitochondrial respiration. Third, despite that our RNA-seq data support the repression of protein synthesis due to ISR and *Eif4ebp1* activation, it remains unclear to what extent the protein synthesis rate is reduced *in vivo* in the *Ant1*^{Tg}/+ compared with the wild-type skeletal muscle. Finally, our studies were primarily focused on the skeletal muscle. Whether and how mitochondrial protein import stress affects the function of other tissues such as the heart and the central nervous system were not addressed in the current study.

STAR★METHODS

Detailed methods are provided in the online version of this paper and include the following:

- KEY RESOURCES TABLE
- RESOURCE AVAILABILITY
  - Lead contact
  - Materials availability
  - Data and code availability
- EXPERIMENTAL MODEL AND SUBJECT DETAILS
  - Mouse models
- METHOD DETAILS
  - Protein extraction, Western blot, and antibodies used for Western blot and immunofluorescence analysis
  - Generation of *Ant1*-transgenic mice
  - Lean mass, home cage activity and exercise endurance tests
  - Mitochondrial isolation and bioenergetic assay
  - Subcellular fractionation and ANT1 sub-mitochondrial localization
  - Muscle histology and immunohistochemistry
  - Electron microscopy
  - RNA-Seq analysis
  - Determination of protein/DNA ratio
  - Proteasomal activity assay
- QUANTITATION AND STATISTICAL ANALYSIS

SUPPLEMENTAL INFORMATION

Supplemental information can be found online at https://doi.org/10.1016/j.isci.2021.103715.

ACKNOWLEDGMENTS

We thank David Mitchell for help on electron microscopy, Siu-Pok Yee (University of Connecticut) for the generation of the *Ant1*-transgenic mice, Don Henderson (University of Rochester) and Christopher Turner for muscle histology, Jushuo Wang for confocal microscopy, SUNY Upstate Medical University Department of Laboratory Animal Resources for animal care, Vanderbilt University Mouse Metabolic Phenotyping Center (MMPC, supported by NIH grants DK059637 and 1S10RR028101-01) for mouse phenotyping, and the

Chen laboratory members for comments on the manuscript. This work was supported by the National Institute of Health (USA) grants AG061204 and AG063499 to X.J.C.

AUTHOR CONTRIBUTIONS

X.W. conducted most experiments. R.T. contributed to muscle histological analysis. F.A.M. processed and analyzed the RNA-seq data. X.J.C. designed the experiments and wrote the paper.

DECLARATION OF INTEREST

The authors declare no competing financial interests.

Received: April 7, 2021
Revised: October 15, 2021
Accepted: December 29, 2021
Published: January 21, 2022

REFERENCES

Adams, C.M., Ebert, S.M., and Dyle, M.C. (2017). Role of ATF4 in skeletal muscle atrophy. Curr. Opin. Clin. Nutr. Metab. Care *20*, 164–168.

Baker, B.M., Nargund, A.M., Sun, T., and Haynes, C.M. (2012). Protective coupling of mitochondrial function and protein synthesis via the eIF2alpha kinase GCN-2. PLoS Genet. *8*, e1002760.

Bao, X.R., Ong, S.E., Goldberger, O., Peng, J., Sharma, R., Thompson, D.A., Vafai, S.B., Cox, A.G., Marutani, E., Ichinose, F., et al. (2016). Mitochondrial dysfunction remodels one-carbon metabolism in human cells. Elife *5*, e10575.

Bonaldo, P., and Sandri, M. (2013). Cellular and molecular mechanisms of muscle atrophy. Dis. Model. Mech. *6*, 25–39.

Bongers, K.S., Fox, D.K., Ebert, S.M., Kunkel, S.D., Dyle, M.C., Bullard, S.A., Dierdorff, J.M., and Adams, C.M. (2013). Skeletal muscle denervation causes skeletal muscle atrophy through a pathway that involves both Gadd45a and HDAC4. Am. J. Physiol. Endocrinol. Metab. *305*, E907–E915.

Boos, F., Kramer, L., Groh, C., Jung, F., Haberkant, P., Stein, F., Wollweber, F., Gackstatter, A., Zoller, E., van der Laan, M., et al. (2019). Mitochondrial protein-induced stress triggers a global adaptive transcriptional programme. Nat. Cell Biol. *21*, 442–451.

Brand, M.D., Pakay, J.L., Ocloo, A., Kokoszka, J., Wallace, D.C., Brookes, P.S., and Cornwall, E.J. (2005). The basal proton conductance of mitochondria depends on adenine nucleotide translocase content. Biochem. J. *392*, 353–362.

Calvani, R., Joseph, A.M., Adhihetty, P.J., Miccheli, A., Bossola, M., Leeuwenburgh, C., Bernabei, R., and Marzetti, E. (2013). Mitochondrial pathways in sarcopenia of aging and disuse muscle atrophy. Biol. Chem. *394*, 393–414.

Carra, S., Alberti, S., Arrigo, P.A., Benesch, J.L., Benjamin, I.J., Boelens, W., Bartelt-Kirbach, B., Brundel, B., Buchner, J., Bukau, B., et al. (2017). The growing world of small heat shock proteins: from structure to functions. Cell Stress Chaperones *22*, 601–611.

Chacinska, A., Koehler, C.M., Milenkovic, D., Lithgow, T., and Pfanner, N. (2009). Importing mitochondrial proteins: machineries and mechanisms. Cell *138*, 628–644.

Chen, H., Vermulst, M., Wang, Y.E., Chomyn, A., Prolla, T.A., McCaffery, J.M., and Chan, D.C. (2010). Mitochondrial fusion is required for mtDNA stability in skeletal muscle and tolerance of mtDNA mutations. Cell *141*, 280–289.

Cohen, S., Nathan, J.A., and Goldberg, A.L. (2015). Muscle wasting in disease: molecular mechanisms and promising therapies. Nat. Rev. Drug Discov. *14*, 58–74.

Coyne, L.P., and Chen, X.J. (2018). mPOS is a novel mitochondrial trigger of cell death - implications for neurodegeneration. FEBS Lett. *592*, 759–775.

Dogan, S.A., Pujol, C., Maiti, P., Kukat, A., Wang, S., Hermans, S., Senft, K., Wibom, R., Rugarli, E.I., and Trifunovic, A. (2014). Tissue-specific loss of DARS2 activates stress responses independently of respiratory chain deficiency in the heart. Cell Metab. *19*, 458–469.

Dorner, A., Schulze, K., Rauch, U., and Schultheiss, H.P. (1997). Adenine nucleotide translocator in dilated cardiomyopathy: pathophysiological alterations in expression and function. Mol. Cell Biochem. *174*, 261–269.

Dubowitz, V., Lane, R., and Sewry, C.A. (2007). Muscle Biopsy: A Pratical Approach, Third edition (Saunders Elsevier).

Ebert, S.M., Dyle, M.C., Kunkel, S.D., Bullard, S.A., Bongers, K.S., Fox, D.K., Dierdorff, J.M., Foster, E.D., and Adams, C.M. (2012). Stress-induced skeletal muscle Gadd45a expression reprograms myonuclei and causes muscle atrophy. J. Biol. Chem. *287*, 27290–27301.

Eisler, S.A., Curado, F., Link, G., Schulz, S., Noack, M., Steinke, M., Olayioye, M.A., and Hausser, A. (2018). A Rho signaling network links microtubules to PKD controlled carrier transport to focal adhesions. Elife *7*. https://doi.org/10.7554/eLife.35907.

Fessler, E., Eckl, E.M., Schmitt, S., Mancilla, I.A., Meyer-Bender, M.F., Hanf, M., Philippou-Massier, J., Krebs, S., Zischka, H., and Jae, L.T. (2020). A pathway coordinated by DELE1 relays mitochondrial stress to the cytosol. Nature *579*, 433–437.

Fox, D.K., Ebert, S.M., Bongers, K.S., Dyle, M.C., Bullard, S.A., Dierdorff, J.M., Kunkel, S.D., and Adams, C.M. (2014). p53 and ATF4 mediate distinct and additive pathways to skeletal muscle atrophy during limb immobilization. Am. J. Physiol. Endocrinol. Metab. *307*, E245–E261.

Gabellini, D., D'Antona, G., Moggio, M., Prelle, A., Zecca, C., Adami, R., Angeletti, B., Ciscato, P., Pellegrino, M.A., Bottinelli, R., et al. (2006). Facioscapulohumeral muscular dystrophy in mice overexpressing *FRG1*. Nature *439*, 973–977.

Gabellini, D., Green, M.R., and Tupler, R. (2002). Inappropriate gene activation in FSHD: a repressor complex binds a chromosomal repeat deleted in dystrophic muscle. Cell *110*, 339–348.

Garaeva, A.A., Kovaleva, I.E., Chumakov, P.M., and Evstafieva, A.G. (2016). Mitochondrial dysfunction induces SESN2 gene expression through Activating Transcription Factor 4. Cell Cycle *15*, 64–71.

Garcia-Cazarin, M.L., Snider, N.N., and Andrade, F.H. (2011). Mitochondrial isolation from skeletal muscle. J. Vis. Exp. *2452*. https://doi.org/10.3791/2452.

Guo, X., Aviles, G., Liu, Y., Tian, R., Unger, B.A., Lin, Y.T., Wiita, A.P., Xu, K., Correia, M.A., and Kampmann, M. (2020). Mitochondrial stress is relayed to the cytosol by an OMA1-DELE1-HRI pathway. Nature *579*, 427–432.

Hunt, R.J., Granat, L., McElroy, G.S., Ranganathan, R., Chandel, N.S., and Bateman, J.M. (2019). Mitochondrial stress causes neuronal dysfunction via an ATF4-dependent increase in L-2-hydroxyglutarate. J. Cell Biol. *218*, 4007–4016.

Ishikawa, F., Akimoto, T., Yamamoto, H., Araki, Y., Yoshie, T., Mori, K., Hayashi, H., Nose, K., and Shibanuma, M. (2009). Gene expression profiling identifies a role for CHOP during inhibition of the mitochondrial respiratory chain. J. Biochem. *146*, 123–132.

Jackson, T.D., Palmer, C.S., and Stojanovski, D. (2018). Mitochondrial diseases caused by dysfunctional mitochondrial protein import. Biochem. Soc. Trans. *46*, 1225–1238.

Jiang, S., Heller, B., Tagliabracci, V.S., Zhai, L., Irimia, J.M., DePaoli-Roach, A.A., Wells, C.D., Skurat, A.V., and Roach, P.J. (2010). Starch binding domain-containing protein 1/genethonin 1 is a novel participant in glycogen metabolism. J. Biol. Chem. *285*, 34960–34971.

Juliana, C.A., Yang, J., Rozo, A.V., Good, A., Groff, D.N., Wang, S.Z., Green, M.R., and Stoffers, D.A. (2017). ATF5 regulates beta-cell survival during stress. Proc. Natl. Acad. Sci. U S A *114*, 1341–1346.

Kang, Y., Stroud, D.A., Baker, M.J., De Souza, D.P., Frazier, A.E., Liem, M., Tull, D., Mathivanan, S., McConville, M.J., Thorburn, D.R., et al. (2017). Sengers syndrome-associated mitochondrial acylglycerol kinase is a subunit of the human TIM22 protein import complex. Mol. Cell *67*, 457–470.e5.

Khan, N.A., Nikkanen, J., Yatsuga, S., Jackson, C., Wang, L., Pradhan, S., Kivela, R., Pessia, A., Velagapudi, V., and Suomalainen, A. (2017). mTORC1 regulates mitochondrial integrated stress response and mitochondrial myopathy progression. Cell Metab. *26*, 419–428.e5.

Kim, E., Rich, J., Karoutas, A., Tarlykov, P., Cochet, E., Malysheva, D., Mamchaoui, K., Ogryzko, V., and Pirozhkova, I. (2015). ZNF555 protein binds to transcriptional activator site of 4qA allele and ANT1: potential implication in Facioscapulohumeral dystrophy. Nucleic Acids Res. *43*, 8227–8242.

Kim, M.J., Bae, S.H., Ryu, J.C., Kwon, Y., Oh, J.H., Kwon, J., Moon, J.S., Kim, K., Miyawaki, A., Lee, M.G., et al. (2016). SESN2/sestrin2 suppresses sepsis by inducing mitophagy and inhibiting NLRP3 activation in macrophages. Autophagy *12*, 1272–1291.

Kirstein-Miles, J., Scior, A., Deuerling, E., and Morimoto, R.I. (2013). The nascent polypeptide-associated complex is a key regulator of proteostasis. EMBO J. *32*, 1451–1468.

Koehler, C.M., Leuenberger, D., Merchant, S., Renold, A., Junne, T., and Schatz, G. (1999). Human deafness dystonia syndrome is a mitochondrial disease. Proc. Natl. Acad. Sci. U S A *96*, 2141–2146.

Krendel, M., Zenke, F.T., and Bokoch, G.M. (2002). Nucleotide exchange factor GEF-H1 mediates cross-talk between microtubules and the actin cytoskeleton. Nat. Cell Biol. *4*, 294–301.

Kuhl, I., Miranda, M., Atanassov, I., Kuznetsova, I., Hinze, Y., Mourier, A., Filipovska, A., and Larsson, N.G. (2017). Transcriptomic and proteomic landscape of mitochondrial dysfunction reveals secondary coenzyme Q deficiency in mammals. Elife *6*. https://doi.org/10.7554/eLife.30952.

Kumar, A., and Shaha, C. (2018). SESN2 facilitates mitophagy by helping Parkin translocation through ULK1 mediated Beclin1 phosphorylation. Sci. Rep. *8*, 615. https://doi.org/10.1038/s41598-017-19102-2.

Laoudj-Chenivesse, D., Carnac, G., Bisbal, C., Hugon, G., Bouillot, S., Desnuelle, C., Vassetzky, Y., and Fernandez, A. (2005). Increased levels of adenine nucleotide translocator 1 protein and response to oxidative stress are early events in facioscapulohumeral muscular dystrophy muscle. J. Mol. Med. *83*, 216–224.

Law, C.W., Chen, Y., Shi, W., and Smyth, G.K. (2014). voom: precision weights unlock linear model analysis tools for RNA-seq read counts. Genome Biol. *15*, R29.

Lee, E.C., Yu, D., Martinez de Velasco, J., Tessarollo, L., Swing, D.A., Court, D.L., Jenkins, N.A., and Copeland, N.G. (2001). A highly efficient *Escherichia coli*-based chromosome engineering system adapted for recombinogenic targeting and subcloning of BAC DNA. Genomics *73*, 56–65.

Lin, Y.F., and Haynes, C.M. (2016). Metabolism and the UPR(mt). Mol. Cell *61*, 677–682.

Liu, Y., Wang, X., Coyne, L.P., Yang, Y., Qi, Y., Middleton, F.A., and Chen, X.J. (2019). Mitochondrial carrier protein overloading and misfolding induce aggresomes and proteostatic adaptations in the cytosol. Mol. Biol. Cell *30*, 1272–1284.

Love, M.I., Huber, W., and Anders, S. (2014). Moderated estimation of fold change and dispersion for RNA-seq data with DESeq2. Genome Biol. *15*, 550.

Lustgarten, M.S., Jang, Y.C., Liu, Y., Muller, F.L., Qi, W., Steinhelper, M., Brooks, S.V., Larkin, L., Shimizu, T., Shirasawa, T., et al. (2009). Conditional knockout of Mn-SOD targeted to type IIB skeletal muscle fibers increases oxidative stress and is sufficient to alter aerobic exercise capacity. Am. J. Physiol. Cell Physiol. *297*, C1520–C1532.

Lustgarten, M.S., Jang, Y.C., Liu, Y., Qi, W., Qin, Y., Dahia, P.L., Shi, Y., Bhattacharya, A., Muller, F.L., Shimizu, T., et al. (2011). MnSOD deficiency results in elevated oxidative stress and decreased mitochondrial function but does not lead to muscle atrophy during aging. Aging Cell *10*, 493–505.

Martensson, C.U., Priesnitz, C., Song, J., Ellenrieder, L., Doan, K.N., Boos, F., Floerchinger, A., Zufall, N., Oeljeklaus, S., Warscheid, B., and Becker, T. (2019). Mitochondrial protein translocation-associated degradation. Nature *569*, 679–683.

Mick, E., Titov, D.V., Skinner, O.S., Sharma, R., Jourdain, A.A., and Mootha, V.K. (2020). Distinct mitochondrial defects trigger the integrated stress response depending on the metabolic state of the cell. Elife *9*. https://doi.org/10.7554/eLife.49178.

Mogk, A., Ruger-Herreros, C., and Bukau, B. (2019). Cellular Functions and mechanisms of action of small heat shock proteins. Annu. Rev. Microbiol. *73*, 89–110.

Morrow, R.M., Picard, M., Derbeneva, O., Leipzig, J., McManus, M.J., Gouspillou, G., Barbat-Artigas, S., Dos Santos, C., Hepple, R.T., Murdock, D.G., and Wallace, D.C. (2017). Mitochondrial energy deficiency leads to hyperproliferation of skeletal muscle mitochondria and enhanced insulin sensitivity. Proc. Natl. Acad. Sci. U S A *114*, 2705–2710.

Nagy, A., Gertsenstein, M., Vintersten, K., and Behringer, R. (2003). Manipulatiing the Mouse Embryo: A Laboratory Manual, Third edition (Cold Spring Harbor Laboratory Press).

Nakazawa, T., Hashimoto, R., Sakoori, K., Sugaya, Y., Tanimura, A., Hashimotodani, Y., Ohi, K., Yamamori, H., Yasuda, Y., Umeda-Yano, S., et al. (2016). Emerging roles of ARHGAP33 in intracellular trafficking of TrkB and pathophysiology of neuropsychiatric disorders. Nat. Commun. *7*, 10594. https://doi.org/10.1038/ncomms10594.

Naresh, N.U., and Haynes, C.M. (2019). Signaling and regulation of the mitochondrial unfolded protein response. Cold Spring Harb. Perspect. Biol. *11*. https://doi.org/10.1101/cshperspect.a033944.

Nargund, A.M., Pellegrino, M.W., Fiorese, C.J., Baker, B.M., and Haynes, C.M. (2012). Mitochondrial import efficiency of ATFS-1 regulates mitochondrial UPR activation. Science *337*, 587–590.

Nikkanen, J., Forsstrom, S., Euro, L., Paetau, I., Kohnz, R.A., Wang, L., Chilov, D., Viinamaki, J., Roivainen, A., Marjamaki, P., et al. (2016). Mitochondrial DNA replication defects disturb cellular dNTP pools and remodel one-carbon metabolism. Cell Metab. *23*, 635–648.

Nunnari, J., and Suomalainen, A. (2012). Mitochondria: in sickness and in health. Cell *148*, 1145–1159.

Ost, M., Keipert, S., van Schothorst, E.M., Donner, V., van der Stelt, I., Kipp, A.P., Petzke, K.J., Jove, M., Pamplona, R., Portero-Otin, M., et al. (2015). Muscle mitohormesis promotes cellular survival via serine/glycine pathway flux. FASEB J. *29*, 1314–1328.

Pacheu-Grau, D., Callegari, S., Emperador, S., Thompson, K., Aich, A., Topol, S.E., Spencer, E.G., McFarland, R., Ruiz-Pesini, E., Torkamani, A., et al. (2018). Mutations of the mitochondrial carrier translocase channel subunit TIM22 cause early-onset mitochondrial myopathy. Hum. Mol. Genet. *27*, 4135–4144.

Pakos-Zebrucka, K., Koryga, I., Mnich, K., Ljujic, M., Samali, A., and Gorman, A.M. (2016). The integrated stress response. EMBO Rep. *17*, 1374–1395.

Patro, R., Duggal, G., Love, M.I., Irizarry, R.A., and Kingsford, C. (2017). Salmon provides fast and bias-aware quantification of transcript expression. Nat. Methods *14*, 417–419.

Poveda-Huertes, D., Matic, S., Marada, A., Habernig, L., Licheva, M., Myketin, L., Gilsbach, R., Tosal-Castano, S., Papinski, D., Mulica, P., et al. (2020). An early mtUPR: redistribution of the nuclear transcription factor rox1 to mitochondria protects against intramitochondrial proteotoxic aggregates. Mol. Cell *77*, 180–188 e189.

Quiros, P.M., Prado, M.A., Zamboni, N., D'Amico, D., Williams, R.W., Finley, D., Gygi, S.P., and Auwerx, J. (2017). Multi-omics analysis identifies ATF4 as a key regulator of the mitochondrial stress response in mammals. J. Cell Biol. *216*, 2027–2045.

Romanello, V., and Sandri, M. (2016). Mitochondrial quality control and muscle mass

maintenance. Front. Physiol. *6*, 422. https://doi.org/10.3389/fphys.2015.00422.

Rugarli, E.I., and Langer, T. (2012). Mitochondrial quality control: a matter of life and death for neurons. EMBO J. *31*, 1336–1349.

Sergushichev, A.A. (2016). An algorithm for fast preranked gene set enrichment analysis using cumulative statistic calculation. bioRxiv, 60012 [Preprint].

Silva, J.M., Wong, A., Carelli, V., and Cortopassi, G.A. (2009). Inhibition of mitochondrial function induces an integrated stress response in oligodendroglia. Neurobiol. Dis. *34*, 357–365.

Statland, J.M., and Tawil, R. (2011). Facioscapulohumeral muscular dystrophy: molecular pathological advances and future directions. Curr. Opin. Neurol. *24*, 423–428.

Topf, U., Wrobel, L., and Chacinska, A. (2016). Chatty mitochondria: keeping balance in cellular protein homeostasis. Trends Cell Biol. https://doi.org/10.1016/j.tcb.2016.03.002.

Tyynismaa, H., Carroll, C.J., Raimundo, N., Ahola-Erkkila, S., Wenz, T., Ruhanen, H., Guse, K., Hemminki, A., Peltola-Mjosund, K.E., Tulkki, V., et al. (2010). Mitochondrial myopathy induces a starvation-like response. Hum. Mol. Genet. *19*, 3948–3958.

Veatch, J.R., McMurray, M.A., Nelson, Z.W., and Gottschling, D.E. (2009). Mitochondrial dysfunction leads to nuclear genome instability via an iron-sulfur cluster defect. Cell *137*, 1247–1258.

Vukotic, M., Nolte, H., Konig, T., Saita, S., Ananjew, M., Kruger, M., Tatsuta, T., and Langer, T. (2017). Acylglycerol kinase mutated in sengers syndrome is a subunit of the TIM22 protein translocase in mitochondria. Mol. Cell *67*, 471–483 e477.

Wang, X. (2001). The expanding role of mitochondria in apoptosis. Genes Dev. *15*, 2922–2933.

Wang, X., and Chen, X.J. (2015). A cytosolic network suppressing mitochondria-mediated proteostatic stress and cell death. Nature *524*, 481–484.

Weidberg, H., and Amon, A. (2018). MitoCPR-A surveillance pathway that protects mitochondria in response to protein import stress. Science *360*. https://doi.org/10.1126/science.aan4146.

West, A.P., Khoury-Hanold, W., Staron, M., Tal, M.C., Pineda, C.M., Lang, S.M., Bestwick, M., Duguay, B.A., Raimundo, N., MacDuff, D.A., et al. (2015). Mitochondrial DNA stress primes the antiviral innate immune response. Nature *520*, 553–557.

Wrobel, L., Topf, U., Bragoszewski, P., Wiese, S., Sztolsztener, M.E., Oeljeklaus, S., Varabyova, A., Lirski, M., Chroscicki, P., Mroczek, S., et al. (2015). Mistargeted mitochondrial proteins activate a proteostatic response in the cytosol. Nature *524*, 485–488.

Zhang, Q., Wu, X., Chen, P., Liu, L., Xin, N., Tian, Y., and Dillin, A. (2018). The mitochondrial unfolded protein response is mediated cell-non-autonomously by retromer-dependent Wnt signaling. Cell *174*, 870–883.e17.

Zhang, Y., Davis, C., Sakellariou, G.K., Shi, Y., Kayani, A.C., Pulliam, D., Bhattacharya, A., Richardson, A., Jackson, M.J., McArdle, A., et al. (2013). CuZnSOD gene deletion targeted to skeletal muscle leads to loss of contractile force but does not cause muscle atrophy in adult mice. FASEB J. *27*, 3536–3548.

Zurita Rendon, O., and Shoubridge, E.A. (2018). LONP1 is required for maturation of a subset of mitochondrial proteins, and its loss elicits an integrated stress response. Mol. Cell Biol. *38*, e00412–e00417.

STAR★METHODS

KEY RESOURCES TABLE

REAGENT or RESOURCE	SOURCE	IDENTIFIER
Antibodies		
Monoclonal mouse anti-ACO2	abcam	Cat. #ab110321; RRID:AB_10863392
Polyclonal rabbit anti-ANT1	Sigma-Aldrich	Cat. #SAB2108761-100UL
Monoclonal rabbit anti-4E-BP1	Cell Signaling	Cat. #9644; RRID:AB_2097841
Monoclonal rabbit anti-Phospho-4E-BP1	Cell Signaling	Cat. #2855; RRID:AB_560835
Polyclonal rabbit anti-eIF2α	Cell Signaling	Cat. #9722; RRID:AB_2230924
Monoclonal rabbit anti-P-eIF2α (Ser51)	Cell Signaling	Cat. #3597; RRID:AB_390740
Monoclonal mouse anti-GAPDH	abcam	Cat. #ab9482; RRID:AB_307272
Polyclonal rat anti-Lamp-1 (WB)	DSHB, The University of Iowa	Cat. #1D4B; RRID:AB_2134500
Polyclonal rat anti-Lamp-2 (WB)	DSHB, The University of Iowa	Cat. #ABL-93; RRID:AB_2134767
Polyclonal rat anti-Lamp-2 (IF)	DSHB, The University of Iowa	Cat. #GL2A7; RRID:AB_528182
Monoclonal rabbit anti-Mdh2 (D8Q5S)	Cell Signaling	Cat. #11908; RRID:AB_2797764
Monoclonal mouse anti-MitoProfileA Total OXPHOS WB antibody Cocktail	abcam	Cat. #ab110411; RRID:AB_2756818
Monoclonal rabbit anti-p70 S6 Kinase (49D7)	Cell Signaling	Cat. #2708; RRID:AB_390722
Monoclonal mouse anti-p-p70 S6 Kinase α (E-5)	Santa Cruz	Cat. #sc-377529
Monoclonal rabbit anti-SDHA	Cell Signaling	Cat. #5839; RRID:AB_10707493
Polyclonal rabbit anti-SMAC	abcam	Cat. #ab8114; RRID:AB_306284
Monoclonal rabbit anti-SQSTM1/p62(D6M5X)	Cell Signaling	Cat. #23214; RRID:AB_2798858
Monoclonal mouse anti-TIM23	BD Biosciences	Cat. #611222; RRID:AB_398754
Monoclonal rabbit anti-Tom20	Cell Signaling	Cat. #42406; RRID:AB_2687663
Polyclonal rabbit anti-Ubiquitin	Cell Signaling	Cat. #3933; RRID:AB_2180538
Chemicals, peptides, and recombinant proteins		
Complete Protease Inhibitor Cocktail	Sigma	Cat. #11697498001
Critical commercial assays		
iTaq Universal SYBR Green Supermix	BIO-RAD	Cat. #1725121
Revert 700 Total Protein Stain	LI-COR	Cat. #926-11021
Proteasome-Glo™ Assay Systems	Promega	Cat. #G8531
AllPrep DNA/RNA/Protein Mini kit	Qiagen	Cat. #80004
Bradford protein assay	Bio-Rad	Cat. #5000006
Experimental models: Organisms/strains		
Ant1-transgenic mouse	Chen lab	https://www.xinjiechenlab.com/
Oligonucleotides		
5′-GTCGAATTCGTATATAAATAAATAAA AGAAAG	This study	ret5F
5′GTCAGACGTCCAA TGTTGCTACTTAAACACTCTTG	This study	ret5R
5′-GTCAGACGTCCCTTGAGAACTAACAC AGAGCAG	This study	ret3F

(*Continued on next page*)

Continued

REAGENT or RESOURCE	SOURCE	IDENTIFIER
5′-GTCAAAGCTTGGTGATATGGGGACAG GAAGGAG).	This study	ret3R
5′-GGATCCCCCGGGCTGCAGGAATTC	This study	BHtoRI
5′-CAATGTTGCTACTTAAACACTCTTG	This study	AntR5
5′-GAGGTCGACGGTATCGATAAGCTTG	This study	XhotoHind
5′-CTTTCCTGGACCCCTGTAAGCTTG	This study	AntR3F
5′-GCTCCGATCATCGTTTAGCAGC	This study	AntR5FP
5′-CAATGTTGCTACTTAAACACTCTTG	This study	AntR5RP (=AntR5)
5′-CACCAGGGCTGCTTTTAACTCTGGTA	This study	GapdhFP
5′-CCTTGACGGTGCCATGGAATTTGC	This study	GapdhRP
Software and algorithms		
ImageJ	National Institutes of Health, USA	https://imagej.nih.gov.ij/
Image Studio	LI-COR	N/A
Deposited data		
RNA-Seq data from 6-month-old Ant1-transgenic skeletal muscle	This study	NCBI Gene Expression Omnibus/Sequence Read Archive (accession number: GSE135584).
Other		
Oxygraph Plus System Version 2.1	Hansatech Instruments	N/A

RESOURCE AVAILABILITY

Lead contact

Further information and requests for resources and reagents should be directed to and will be fulfilled by the Lead Contact, Xin Jie Chen (chenx@upstate.edu).

Materials availability

All unique/stable reagents generated in this study are available from the Lead Contact without restriction.

Data and code availability

All software used in this study is publicly available, and there was no code generated as part of this study. The small datasets generated as part of this study are either present as a supplemental table or will be made available from the corresponding author on request. All raw FastQ files and processed read alignment count data from the RNA-Seq experiments have been deposited into the NCBI Gene Expression Omnibus/Sequence Read Archive (accession number: GSE135584). Any additional information required to reanalyze the data reported in this paper is available from the lead contact upon request.

EXPERIMENTAL MODEL AND SUBJECT DETAILS

Mouse models

The following mouse line was generated and used in this study: *Ant1*-transgenic mice in the C57BL6N genetic background.

METHOD DETAILS

Protein extraction, Western blot, and antibodies used for Western blot and immunofluorescence analysis

50-100 mg of muscle tissues were homogenized in 0.3 ml of ice-cold RIPA buffer (20 mM Tris-HCl, pH7.4; 150 NaCl; 1 mM EDTA, pH7.4; 1% Triton-X100; 1% sodium deoxycholate; 0.1% SDS) added with Complete Mini protease inhibitor cocktail. Cell debris was removed by centrifugation at 13,000 rpm for 3 minutes at

4°C. 30-50 μg of the muscle lysates were used for SDS-PAGE and western-blot analysis. Antibodies used in this study are listed in the key resources table.

Generation of *Ant1*-transgenic mice

The *Ant1* transgene was prepared by recombineering according to Lee et al. (Lee et al., 2001). Briefly, genomic sequences corresponding to *Ant1* 5′ upstream and 3′ downstream genomic sequence were prepared by PCR using primer pairs ret5F and ret5R, and ret3F and ret3R. The 5′ and 3′ mini-arms were digested with *Eco*RI and *Aat*II, and *Hin*dIII and *Aat*II, respectively, and then inserted into pSK+. The mini-arm vector was then digested with *Aat*II, treated with phosphatase, and then electroporated into EL350 together with a BAC clone, RP24-108A1, which contains the entire *Ant1* genomic sequence, to retrieve Ant1 genomic sequence from the BAC by gap repair. The retrieved Ant1 genomic sequence is 13.7 kb in size containing all 4 exons together with 4.2 kb and 4.96 kb of 5′ up- and 3′ down-stream sequences, respectively. The *Ant1* transgene fragment was released from the plasmid by *Not*I and *Kpn*I digestion, fractionated by agarose gel electrophoresis, column purified and resuspended in 10 mM Tris, pH8.0.

Ant1-transgenic mice were generated according to Nagy et al. (Nagy et al., 2003). Briefly, four to 6-week-old C57BL6j females were superovulated by first administration of 5 IU of pregnant mare serum (PMS) and 44 to 46 hour later with 5 IU human chorionic gonadotropins (HCG). The females are then mated with C57BL6j stud males. Fertilized one-cell embryos were collected from the oviduct the next day and maintained in KSOM medium in an air/CO_2 incubator at 37°C until use. Purified Ant1 genomic fragment were diluted to approximately 1 ng/μl and then microinjected into the pronuclei of the one-cell embryos. Injected embryos were implanted into the oviducts of 0.5 days *post coitium* pseudopregnant females for subsequent development *in utero*. Transgenic mice were identified by PCR using genomic DNA prepared from ear notch as template. Two primer pairs specific to the 5′ and 3′ end of the *Ant1* transgene were used for genotyping. Primer pair BHtoRI and Ant R5, corresponds to the 5′ will identify a fragment of 515 bp, and a second pair of primers, XhotoHind and AntR3F will detect a fragment of 432 bp specific to the 3′ end of the transgene. Founder animals were then mated with C57BL6NTac mice to establish and maintain the transgenic line. All the animal experiments have been approved by the Institutional Animal Care and Use Committee (IACUC) of the State University of New York Upstate Medical University. The experiments were performed using age-matched and mostly littermate controls. The animals were fed with a regular chow diet *ad libitum* and were housed at an ambient temperature. Food and water were placed at a low and reachable position for the *Ant1*-transgenic mice over one-year-old.

Quantitative PCR was used to estimate the copy number of the *Ant1* transgene. Total DNA was extracted from 50 mg of mouse tail tissue and 10 ng of DNA was used for qPCR with the primers AntR5FP and AntR5RP that amplify a fragment of 191 bp in the *Ant1* gene. The *Gapdh* gene was used as an internal reference gene.

Lean mass, home cage activity and exercise endurance tests

Lean mass and home cage activity were measured by quantitative magnetic resonance and Promethion metabolic caging respectively at Vanderbilt University Mouse Metabolic Phenotyping Center. Exercise endurance was measured with an Exer 3/6 Treadmill (Columbus Instruments) by determining the maximum distance and speed of the animals before exhaustion. The animals were trained for at least two sessions before the tests.

Mitochondrial isolation and bioenergetic assay

Two pairs of unanesthetized mice at the age of 4- and 14-month-old were decapitated using a guillotine. Hindlimb muscle mitochondria were isolated according to Garcia-Cazabin et al. (Garcia-Cazarin et al., 2011). Oxygen consumption rates were measured using an Oxygraph Plus oxygen electrode (Hansatech Instruments Ltd), with 150 μg mitochondria, 5 mM glutamate, 2.5 mM malate, 150 μM ADP. Oligomycin (5 μg/ml) was added to establish state-4 respiration. For measuring complex II driven respiration, 5 mM of succinate was used as substrates and 5 μM rotenone was added to inhibit respiratory complex I. Respiratory control ratio was established by dividing state-3 respiratory rate with oligomycin-inhibited respiratory rate.

Subcellular fractionation and ANT1 sub-mitochondrial localization

Muscle homogenates were separated into mitochondrial and cytosolic fractions after centrifugation at 10,500 g for 10 minutes. The isolated mitochondria were resuspended in an isotonic buffer lacking BSA (75 mM sucrose, 215 mM mannitol, 1 mM EGTA in 20 mM HEPES-KOH pH 7.4). Proteinase K protection assay was performed under hypotonic conditions (20 mM HEPES-KOH pH7.4, 1 mM EGTA). 40 μg of mitochondria were treated with proteinase K at the indicated concentrations for 30 minutes at room temperature and quenched with 5 mM PMSF on ice for 10 minutes. Where indicated, mitochondria were lysed with 1% Triton X-100 for 30 minutes on ice. The proteins were then dissociated with Laemmli buffer before being loaded onto the SDS-PAGE gel for Western blotting.

Muscle histology and immunohistochemistry

Standard procedures were followed for H&E, Trichrome, NADH, SDH and COX activity staining. Two pairs of *Ant1*^{Tg}/+ and control mice at 12 and 20 months of age were used for the determination of lesser diameter and variability coefficient of quadriceps muscle fibers after H&E staining. Lesser diameter is defined as the maximum diameter across the lesser aspect of the muscle fiber (Dubowitz et al., 2007). 13-43 sections from each muscle were examined and images of muscle fibers were acquired using a 40X objective. Variability coefficient is calculated as Standard Deviation X 1000/Mean Fiber Diameter. For immunofluorescence microscopy, muscle sections of 10 μm thickness were fixed and permeabilized with 100% methanol at -20°C for 15 minutes, rinsed in PBS, treated in blocking buffer (1XPBS/5% Normal Goat Serum/0.3% Triton X-100) for one hour at room temperature, followed by incubation with anti-Lamp2 antibody at 4°C overnight. The specimens were then washed in 1XPBS/0.1% Tween 20 before being probed with an Alexa Fluor 488-conjugated anti-rat IgG (H+L) antibody for one hour at room temperature. After washing with 1XPBS/0.1% Tween 20, the tissue samples were mounted with ProLong Diamond Antifade Mountant with DAPI (#P36962, Invitrogen), and were visualized using a Leica SP8 confocal microscope.

Electron microscopy

3-4 ultrathin sections of fresh quadriceps muscle samples from two *Ant1*^{Tg}/+ mice and their littermate controls at the age of one and two years old were fixed in 4% glutaraldehyde/0.1 M cacodylate buffer, pH7.2 at room temperature for two hours, and postfixed with 1% osmium tetroxide/0.1 M cacodylate buffer, pH7.2 at room temperature for one hour. The specimens were dehydrated in 50%, 70%, 90%, 100% ethanol and propylene oxide, before being embedded in Luft's Araldite 502 embedding medium (Electron Microscopy Sciences, Hatfield, PA) and cut into thin sections. The ultrathin sections were then stained with ethanolic uranyl acetate and Reynold's lead citrate (Polysciences). The samples were examined with a JOEL JEM1400 transmission electron microscope and images were acquired with a Gaten DAT-832 Orius camera.

RNA-Seq analysis

Total RNA was extracted from snap-frozen quadriceps muscles (n=4/genotype/sex) using RNeasy mini kit (Qiagen). The quality of total RNA was validated by Bioanalyzer (Agilent Technologies). Approximately 1 μg of RNA per sample was used to construct the cDNA library using TruSeq stranded mRNA library prep kit (Illumina). The cDNA libraries were quantitated using KAPA library quantification kit for Illumina platforms (Kapa Biosystems). The individual indexed libraries were diluted to 4 nM and pooled in equal quantity, denatured before loading onto the Illumina NextSeq 500. The sequencing was run as paired-end reads (2 × 75 bp per read) with a targeted depth of 60 million paired-end reads per sample. Sequence samples were then aligned and quantified with the Salmon algorithm (Patro et al., 2017) using default parameters in RaNA-seq. Differential expression analysis was performed using a one-way analysis of variance (ANOVA) to test the main effect of genotype using both limma (Law et al., 2014) following quantile normalization and DESeq2 (Love et al., 2014). This yielded a total of 2076 and 2654 significant genes at a *q*-value cutoff of 0.01, respectively. These lists were subjected to volcano plot visualization and hierarchical clustering analysis. In addition to single findings, we also tested for Gene Set Enrichment Analysis (GSEA) using a rapid modified algorithm (Sergushichev, 2016), and displayed the top 20 Pathways and Gene Ontologies in graphical and tabular form.

For the analysis of potential sequence variations in Ant1 transcripts, raw FASTQ files were imported into Partek Flow, adapters trimmed, and the BWA aligner used for alignment to the mouse Ant1 NCBI Reference sequence (accession NM_007450.5). Notably, this sequence includes exactly 140 bases upstream

of the ATG start codon of Ant1. After alignment, consensus sequences were generated using the iVar algorithm and exported to Sequencher for realignment and examination of possible sequence changes. We also used Samtools and LoFreq to probe for possible sequence changes in any of the reads using default variant calling settings in each algorithm. Overall, we found no variants in the *Ant1* transcripts in Samtools in any sample. Only extremely rare base changes were identified in LoFreq, with no mice with mutations occurring in 5% of the reads.

Determination of protein/DNA ratio

DNA and proteins were extracted from approximately 30 mg of quadriceps muscles using AllPrep DNA/RNA/Protein Mini kit. DNA concentrations were determined by Thermo Scientific NanoDrop 2000c spectrophotometer. Protein concentrations were determined by Bradford protein assay. Relative protein contents in the muscles were calculated after normalizing by total amount of DNA.

Proteasomal activity assay

Quadriceps muscle samples (1 mg) were sonicated in PBS plus EDTA (5 mM, pH 7.4) buffer three times for 5 seconds with 25 seconds intervals on ice. After the removal of cell debris by centrifugation, protein concentration of the soluble fractions was determined by Bradford assay. 10 μg of the muscle lysates were used for determining proteasome-associated chymotrypsin-like activity with the Proteasome-Glo^{TM} Assay Systems. Luminescence signals were detected with the SpectraMax i3x Multi-Mode Microplate Reader (Molecular Devices) between 10–30 minutes at room temperature after the addition of luminogenic substrates. The chymotrypsin-like activity was calculated by subtracting MG132 (50 μM)-inhibited activities from total activity.

QUANTITATION AND STATISTICAL ANALYSIS

Results in Figures 1C, 1G, 1H, 2D–2G, 5C, 5F–5H, 6A, 6W, S2C–S2G, S3B, S5C, S6B, S7D, S7E, S7I, S7K and S7N are given as mean ± SEM. Results in 1I, 2H, 2I are presented as mean ± S.D. *P* values were calculated by unpaired Student's *t* test with two-tailed distribution and two-sample unequal variance. The ''n'' in these experiments represents the number of mice used. In Figures 2H and 2I, the data represent eight measurements from two pairs of *Ant1*$^{Tg/+}$ mice and littermate controls. In Figures 4 and S6, one-way analysis of variance (ANOVA) was used in RNA-seq analysis to test the main effect of genotype using both limma following quantile normalization and DESeq2. A *q*-value cutoff of 0.01 was used to identify genes that are differentially expressed in transgenic and wild type muscles.